iScience

Article

Melanocortin 4 receptor-expressing neurons in the lateral stripe of the striatum regulate affect and motor control

Graphical abstract

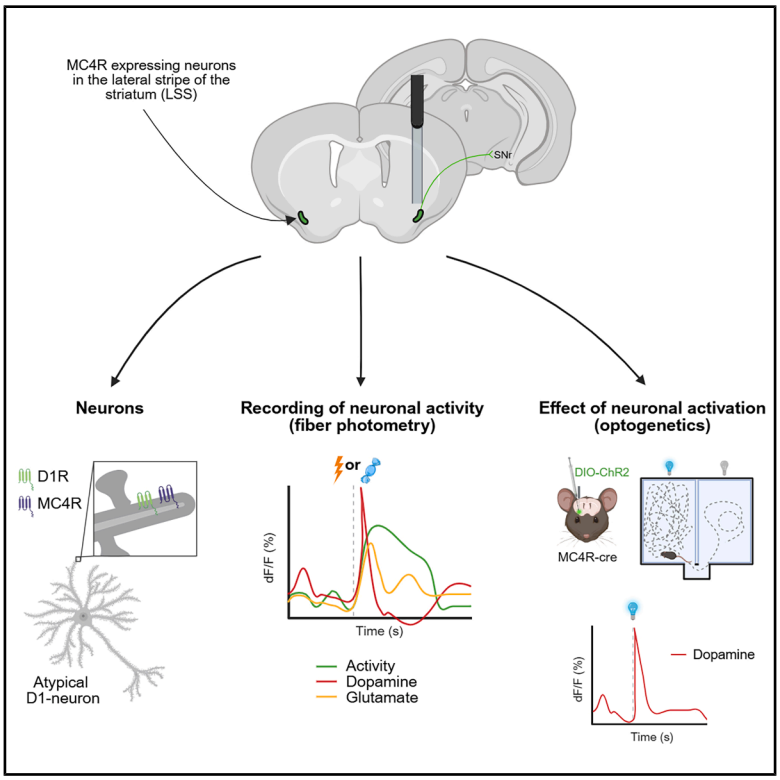

Highlights

- MC4 receptor (MC4R) expression is enriched in the lateral stripe of the striatum (LSS)
- MC4R-LSS neurons are activated by both rewarding and aversive stimuli
- In the LSS, MC4R neuronal activity and glutamate release correlates with movement
- Activation of MC4R-LSS neurons is reinforcing, and induces locomotion and dopamine release

Authors

Johan Sköld, Gisela Paola Lazzarino, Myra Nett, Joost Wiskerke, David Engblom

Correspondence

david.engblom@liu.se

In brief

Molecular biology; Neuroscience

Sköld et al., 2025, iScience *28*, 112456
May 16, 2025
https://doi.org/10.1016/j.isci.2025.112456

CellPress

iScience

CellPress
OPEN ACCESS

Article

Melanocortin 4 receptor-expressing neurons in the lateral stripe of the striatum regulate affect and motor control

Johan Sköld,[1,2] Gisela Paola Lazzarino,[1,2] Myra Nett,[1] Joost Wiskerke,[1] and David Engblom[1,3,*]
[1]Center for Social and Affective Neuroscience, Department of Biomedical and Clinical Sciences, Linköping University, Linköping, Sweden
[2]These authors contributed equally
[3]Lead contact
*Correspondence: david.engblom@liu.se
https://doi.org/10.1016/j.isci.2025.112456

SUMMARY

The dopaminergic system is crucial for affect regulation. Melanocortin 4 receptors (MC4R) in the ventral striatum have been shown to be necessary for establishing aversive states. Here, we functionally characterize MC4R-expressing striatal neurons in mice. MC4Rs were enriched in atypical dopamine receptor 1 (D1) neurons in the lateral stripe of the striatum (LSS), an understudied area in the ventrolateral striatum. Fiber photometry recordings showed that MC4R neuron activity and local dopamine release in the LSS increased in response to both rewarding and aversive stimuli. Moreover, MC4R neuronal activity and glutamate release in the LSS correlated with body movement. Optogenetic activation of MC4R-LSS neurons was rewarding in a real-time place preference test and a self-stimulation paradigm, increased locomotor activity, and induced striatal dopamine release. Collectively, our findings suggest that MC4R-LSS neurons are activated by stimuli of both rewarding and aversive character and that they induce positive affect, dopamine release and locomotion.

INTRODUCTION

Understanding the neurobiological mechanisms driving negative affect is crucial for developing new treatment strategies for a wide variety of pathological conditions, from major depressive disorder to negative affect in inflammatory diseases. The dopaminergic system, including the striatum, is involved in the induction of negative affect.[1–5] The melanocortin system has been identified as a key regulator of motivated behaviors within the ventral striatum.[6] It has been shown that signaling through the melanocortin 4-receptor (MC4R) in dopamine receptor 1 (D1) neurons of the nucleus accumbens (NAc) is increased in anhedonia.[7] Moreover, our laboratory has previously demonstrated that MC4Rs in the striatum are crucial for establishing aversive responses. We found that mice lacking MC4Rs were seeking, instead of avoiding, environments associated with aversive stimuli, indicating that they found the aversive stimuli rewarding. When MC4R expression was rescued in the striatum, or in D1 expressing neurons, of MC4R −/− mice, the mice displayed normal responses to aversive stimuli. This suggests that MC4Rs in striatal D1 neurons work as a switch controlling the valence of aversive stimuli,[8] but the mechanisms behind this "switching" are unclear and the identity of the MC4R expressing neurons in the striatum has not yet been fully elucidated. A brain-wide mapping study in mice suggests that MC4R expressing neurons are enriched in the lateral stripe of the striatum (LSS),[9] an often-overlooked structure located in the ventrolateral striatum. Interestingly, recent single-cell RNA sequencing (scRNA-seq) studies indicate that the LSS is also enriched in a population of neurons that does not cluster with the classic D1-or D2 neurons. These cells are defined alternately as "hybrid D1 neurons", "eccentric spiny projection neurons", or "atypical D1 neurons".[10–13]

Here, we characterized the identity and functions of the MC4R-expressing neurons located in the LSS, showing that these neurons share characteristics with atypical D1 neurons. Using transgenic mice and optical techniques, such as *in vivo* calcium imaging and optogenetics, combined with behavioral analysis, we show that MC4R-LSS neurons are activated by both rewarding and aversive stimuli and that their activation is rewarding.

RESULTS

MC4R is expressed by atypical medium spiny neurons in the lateral stripe of the striatum

To visualize the localization of MC4R-expression in the striatum, we crossed MC4R-cre mice with mice carrying a floxed tdTomato gene. We found that the MC4R-expression is enriched in the LSS, while expression in the rest of the striatum is sparse (Figure 1A). Expression of MC4R in adult mice was confirmed using *in situ* hybridization (Figure S1A). In a mouse expressing GFP under the MC4R-promoter and tdTomato under the D1-promoter, we found that the majority of MC4R-LSS neurons also

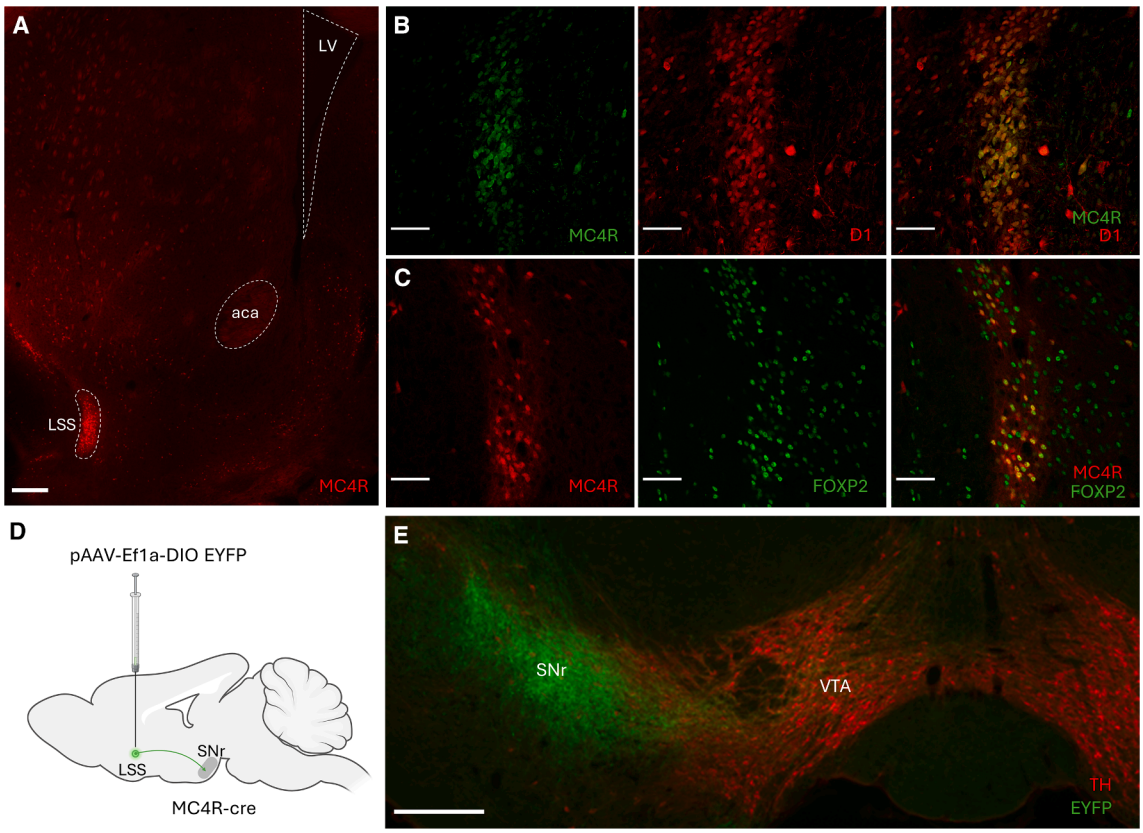

Figure 1. MC4R is expressed by substantia nigra-projecting atypical D1-neurons in the lateral stripe of the striatum

(A) Coronal section of an MC4R-cre, tdTomato-mouse showing the expression pattern of MC4R in the striatum. MC4R-expressing neurons are enriched in the lateral stripe of the striatum (LSS) and sparse in the rest of the striatum.

(B) Confocal picture showing colocalization (right) of MC4R- (green) and D1-expression (red) in the LSS of a mouse expressing GFP under the MC4R-promoter and tdTomato under the D1-promoter.

(C) MC4R-LSS neurons co-express FOXP2 (right), a marker for atypical D1-neurons. MC4R-cre-tdTomato (red) and FOXP2 (green) are expressed by the same neurons.

(D) Schematic depicting the site of the virus injection and the major projection from LSS to substantia nigra pars reticulata (SNr). MC4R-cre mice were injected with pAAV-Ef1a-DIO EYFP in LSS.

(E) Representative image of the projections of LSS-MC4R neurons to SNr. Fibers from MC4R-LSS neurons are shown in green, and tyrosine hydroxylase (TH)-expressing cells in red. Scale bars 200 μm (A and E) and 50 μm (B and C). LV, lateral ventricle; aca, anterior commissure; VTA, ventral tegmental area.

expressed D1-receptors (Figure 1B). Since the LSS is known to harbor atypical D1-neurons with high FOXP2-expression,[10–13] we counterstained sections from MC4R-tdTomato brains for FOXP2. We found high FOXP2-expression in the LSS, with 96.4% (1207/1252) of MC4R-LSS neurons expressing FOXP2 (Figure 1C). To investigate projection patterns of MC4R-LSS neurons, we injected a cre-dependent EYFP vector into the LSS of MC4R-cre mice. Projection mapping of these mice showed dense projections to the substantia nigra pars reticulata, among other brain areas (Figures 1D, 1E, and S1B–S1F). To investigate if the MC4R-LSS neurons receive afferents from POMC-neurons in the arcuate nucleus of the hypothalamus (ARC; the primary source of the MC4R-agonist α-melanocyte stimulating hormone, α-MSH), we injected a cre-dependent EYFP vector in the ARC of POMC-cre mice. Labeled fibers were seen in the medial NAc shell, but not in the LSS, indicating that MC4R-LSS neurons do not receive direct synaptic α-MSH inputs from the ARC (Figure S2). Altogether, these results indicate that the MC4R is expressed by atypical D1-neurons in the LSS.

MC4R-LSS neurons are activated by aversive foot shocks

Since the MC4R has been reported to be necessary for aversive signaling, we measured how the MC4R-LSS neurons respond to aversive stimuli. To test this, we injected a viral vector carrying a cre-dependent genetically encoded calcium indicator (GCaMP8m) into the LSS of MC4R-cre mice and implanted an optic fiber over the LSS, allowing us to measure intracellular calcium as a proxy for neural activity with fiber photometry. We found an increase in firing of MC4R-LSS neurons during exposure to an aversive foot shock (Figures 2A–2D). In contrast, no apparent change in intracellular calcium was observed in response to the conditioned tone predicting the shock during

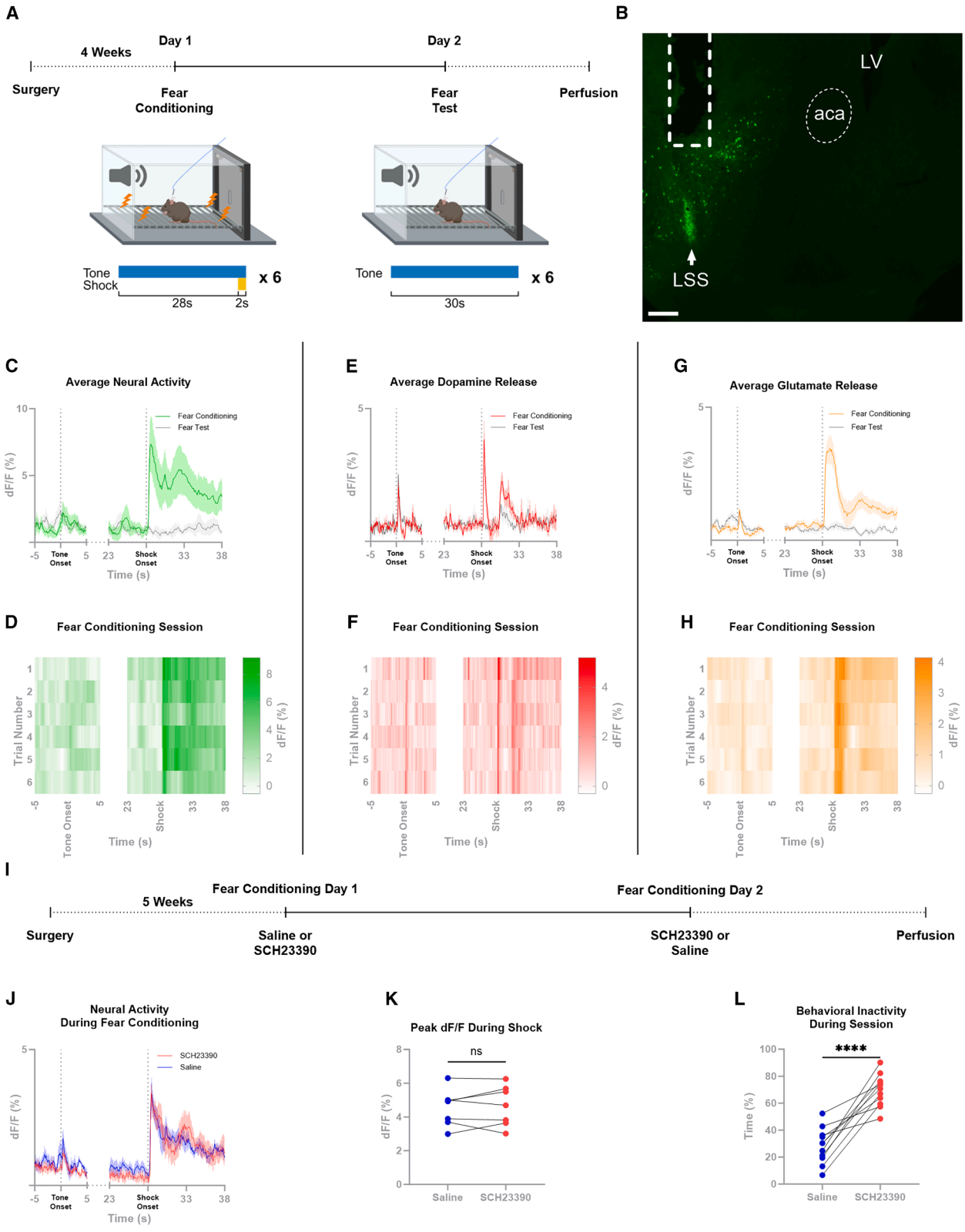

(legend on next page)

the acquisition session or the subsequent day when the shock was omitted (Figure 2C).

Neurotransmitter release in the LSS during aversive fear conditioning

Two of the primary afferent neurotransmitters to striatal medium spiny neurons are dopamine from midbrain dopaminergic neurons and glutamate from the cortex and the thalamus.[14,15] In this study, we aimed to elucidate the afferent signals affecting MC4R-LSS neurons by measuring the dopamine and glutamate release in the LSS during a fear conditioning paradigm, using fiber photometry, the dopamine sensor dLight1.2, and the glutamate sensor SF_iGluSnFR. To increase signal-to-noise ratio for the cre-dependent glutamate sensor, D1-cre instead of MC4R-cre animals were used. We found a robust and reproducible increase in dopamine release in response to both foot shocks and the conditioned tone predicting foot shocks (Figures 2E and 2F), while glutamate was released primarily in response to the shock (Figures 2G and 2H). On the test day, when the shock was omitted, we detected robust release of dopamine and a small increase in glutamate release in response to the tone onset. The unexpected absence of the shock did not result in altered release of either of these two neurotransmitters (Figures 2E and 2G). To explore the specificity of dopamine release in response to aversive foot shocks within the LSS, we performed fear conditioning while measuring dopamine release from the NAcC. We found that dopamine was released in the NAcC in response to both aversive foot shocks and their predictive cues (Figures S3A and S3B). These results indicate that the dopamine dynamics in the LSS are similar to those in the NAcC. To test if dopamine signaling via D1-receptors is necessary for the activity of the MC4R-LSS neurons, we compared shock-induced calcium transients with and without D1-antagonism. Blocking D1-receptors did not decrease the size of the shock-induced peak in neural activity (t_6 = 0.56, ns), while it decreased the movement of the animal during the session, proving pharmacological effect (t_{10} = 7.17, $p < 0.001$; Figures 2I–2L). These results suggest that MC4R-LSS neurons are activated by aversive foot shocks and that this increase is not driven by D1-receptor signaling on the neurons.

In the LSS, MC4R-neural activity and glutamate release, but not dopamine release, are correlated to movement

During the fear conditioning test, we observed a striking correlation between the neural activity and the movement of the animal, measured in pixels changed per video frame, which includes all movements done by the animal (Figure 3A). A cross-correlation of the signals revealed a high correlation with virtually no time-shift (t_5 = 9.62, $p < 0.001$; Figure 3B), indicating that MC4R-LSS neurons are a part of the movement selection and initiation system. To investigate whether the movement correlation is specific to MC4R-LSS neurons, we measured GCaMP6s signal from non-specific neurons in the lateral part of the NAc core (NAcC) during the same conditions. We found that the neural activity measured from all neurons in the NAcC is also highly correlated to the movement of the animal (Figure S3C), indicating that the correlation between neural activity and body movements is not specific to MC4R-neurons nor the LSS. In contrast to the neural activity of MC4R-LSS neurons, dopamine release measured with fiber photometry was not correlated to the movement of the animal when measured in either the LSS or the NAcC (t_6 = 0.86, ns; Figures 3C, 3D, and S3D), suggesting that the neural activity of MC4R-LSS neurons is not directly driven by dopamine. Glutamate release in the LSS shared dynamics with MC4R-LSS-neural activity during fear conditioning and was also correlated to animal movement (t_9 = 2.63, p = 0.03; Figures 3E and 3F), suggesting that glutamate is the fast driver of MC4R-LSS neurons.

Figure 2. MC4R-LSS neurons are activated by aversive foot shocks in a D1-independent manner

(A) Timeline of experiments.

(B) Representative picture of GCaMP8m-expression and fiber placement in the lateral stripe of the striatum (LSS) of an MC4R-cre mouse. Fiber tract and anterior commissure (aca) marked with dashed line; LSS marked with arrow. LV, lateral ventricle. Scale bar 200 μm.

(C) GCaMP8m signal measured with fiber photometry from MC4R-LSS neurons shows activation of MC4R-LSS neurons in response to aversive shocks, but not to the onset of the predictive tone cue. No change in neural activity was seen in response to shock omission in the fear test on day 2. Mean and SEM from 6 mice, 6 trials per mouse.

(D) Heatmap of the data shown in (C) but split out per trial showing that the neural response is similar across all trials. Each row in the heatmap represents the mean from 6 mice.

(E) Dopamine measurements from the LSS during the same behavioral paradigm as in (C). Dopamine is released in the LSS in response to both the aversive foot shocks and their predictive tone cues. No clear change in dopamine release was seen in response to shock omission in the fear test on day 2. Mean and SEM from 7 mice, 6 trials per mouse.

(F) Heatmap of the data shown in (E) but split out per trial showing that the tone-induced dopamine release develops during the session. Each row in the heatmap represents the mean from 7 mice.

(G) iGluSnFR-measurements of glutamate release onto D1-expressing neurons in the LSS during fear conditioning. Glutamate is released onto D1-expressing neurons in response to the aversive foot shock. A small release can be seen in response to the tone onset. Mean and SEM from 10 mice, 6 trials per mouse.

(H) Heatmap of the data shown in (G), but split out per trial, showing that the shock-induced glutamate release is similar across trials and that the tone-induced release is developed within the session. Each row in the heatmap represents the mean from 10 mice.

(I) Timeline of the crossover experiment testing if shock-induced activity of MC4R-LSS neurons is D1-dependent.

(J) Group mean peri-event traces (± SEM) from the experiment shows a robust increase in neural activity in response to the foot shock after both saline-injection and pretreatment with the D1-antagonist SCH23390 (0.2 mg/kg; n = 7).

(K) Mean peak size during the shock for each animal showing that SCH23390 does not affect the shock-induced neural response (n = 7, paired two-tailed t-test).

(L) Analysis of the inactivity time during the sessions showing that mice spend significantly more time inactive after SCH23390 injection compared to saline injection (n = 11, paired two-tailed t-test). ***$p < 0.001$.

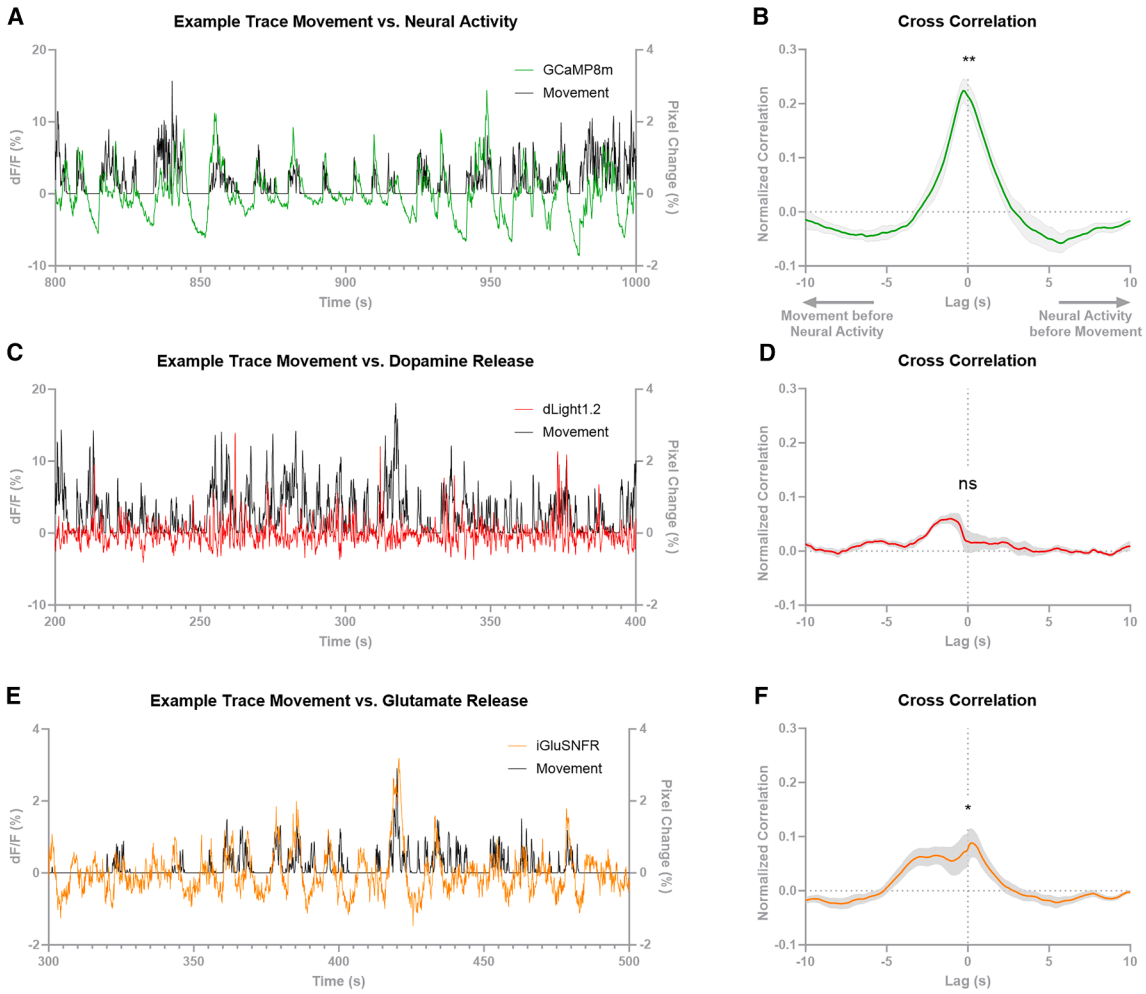

Figure 3. MC4R-LSS-neural activity is correlated to body movement

(A) Part of an example trace of MC4R-lateral stripe of the striatum (LSS) neuronal activity measured with fiber photometry and the calcium sensor GCaMP8m plotted together with body movement of the animal (measured as pixel change per video frame during the fear test) showing a correlation between the two measurements.

(B) A cross-correlation of neural activity and movement shows a positive correlation with almost no time shift. R-values at lag 0 are significantly different from 0 (n = 6, one sample t-test). Data are expressed as mean ± SEM.

(C) Part of an example trace of dopamine release in the LSS measured with fiber photometry and the dopamine sensor dLight1.2 plotted together with body movement of the animal showing that dopamine release in the LSS is not correlated to animal movement.

(D) A cross-correlation of dopamine release and movement showing that dopamine release is not correlated to the movement of the animal (n = 7, one sample t-test). Data are expressed as mean ± SEM.

(E) Part of an example trace of glutamate release onto D1-LSS-neurons measured with fiber photometry and the glutamate sensor iGluSnFR plotted together with body movement of the animal showing a correlation between glutamate release and movement of the animal.

(F) A cross correlation of glutamate release and movement shows a correlation with no time shift 0 (n = 10, one sample t-test). Collectively, these data indicates that MC4R-LSS neurons are mainly driven by glutamate, not dopamine, in the short term. Data are expressed as mean ± SEM. *p < 0.05; **p < 0.01.

MC4R-LSS neurons are activated by sugar pellet consumption

Having established the responsiveness of MC4R-LSS neurons to aversive foot shocks, we further investigated their response to rewarding stimuli and compared it with aversion-induced neural activation. In a Pavlovian conditioning paradigm, food-restricted mice with a genetically encoded calcium indicator (GCaMP8m) and an optic fiber placed above the LSS were trained using a tone predicting the delivery of a sugar pellet. MC4R-LSS neurons were activated by sugar pellet consumption but not by the predictive tone (Figures 4A–4C, Video S1). Unpredicted and predicted pellets generated equal responses, and the omission of a predicted pellet did not affect the neural activity in any direction (Figures S4A and S4B). To compare the magnitude of neural responses induced by rewarding and aversive stimuli and their cues, we exposed the trained animals to a combined session consisting of 10 sugar pellet deliveries followed by 10 aversive foot shocks (Figures 4B–4E). For both the sugar pellet trials (t_5 = 0.45,

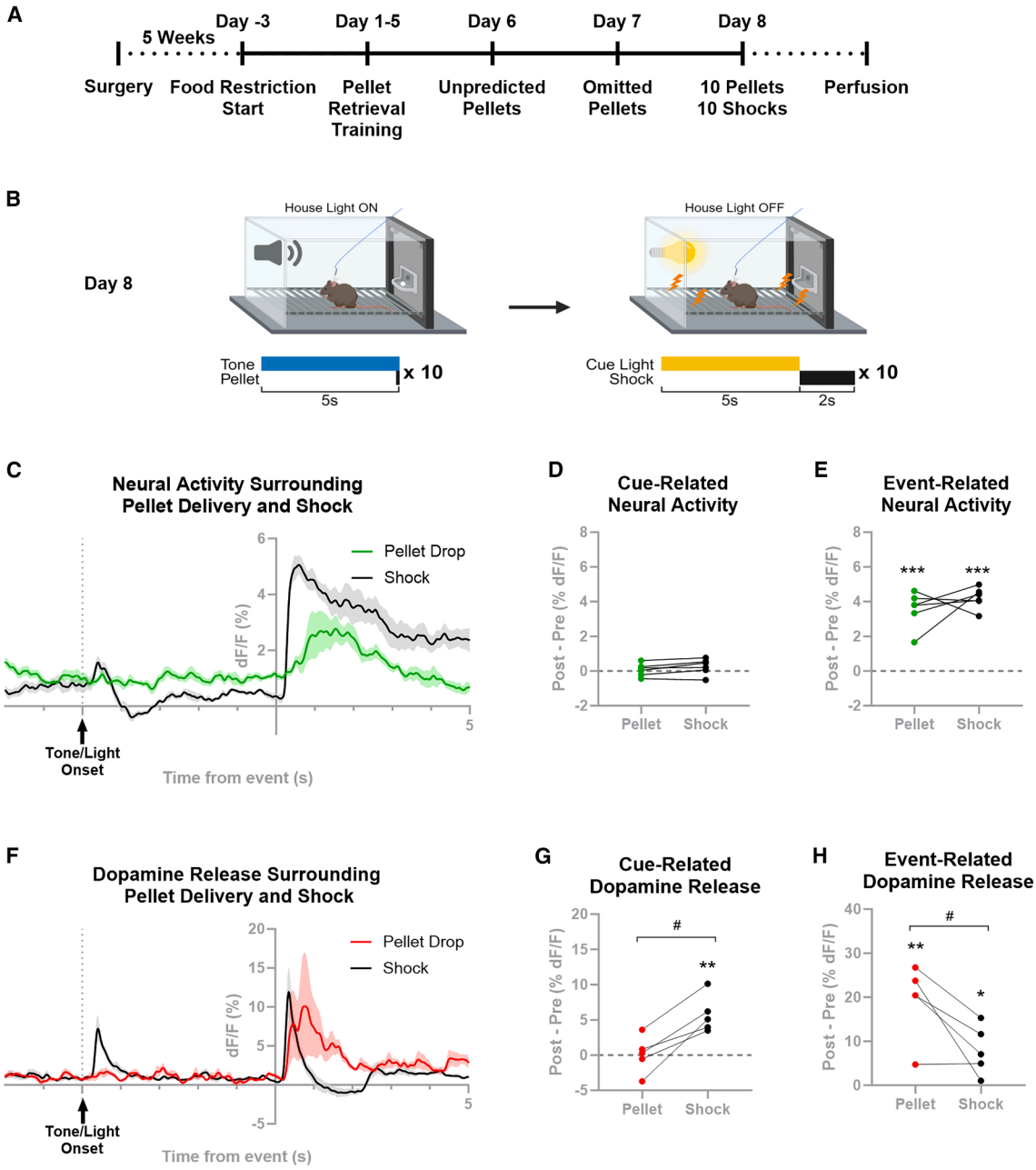

Figure 4. MC4R-LSS neurons are activated, and dopamine is released in the LSS in response to sugar pellet consumption

(A) Timeline of the experiment.

(B) Trial structure of the combined reward and aversion session on day 8.

(C) Mean ± SEM dF/F for GCaMP8m signal from the combined reward and aversion session on day 8 (mean from 10 trials for each stimulus per animal, $n = 6$ mice).

(D) Peak neural activity 1s after cue onset minus peak signal 1s before cue onset showing that neither the cue predicting pellet delivery nor the cue predicting foot shock induced a neural response.

(E) Maximal dF/F during 2s surrounding pellet consumption and 2s following the onset of the foot shock, minus respective peak signal during 2s pre-cue baseline. Neural activity is increased by both sugar pellet consumption and by foot shock, with responses of a similar magnitude in both trial types.

(F) Dopamine measurements (dLight1.2) from the LSS during the same paradigm as in (C). Dopamine is released in response to both pellet consumption and foot shock (mean from 10 trials for each stimulus per animal, $n = 5$ mice, data expressed as mean ± SEM).

(G) Maximal dLight1.2 signal 1s after cue onset minus maximal signal 1s before cue onset showing that dopamine is released in the LSS in response to a cue predicting an aversive foot shock but not in response to a cue predicting sugar pellet delivery.

(legend continued on next page)

ns) and the foot shock (t_5 = 1.36, ns), no increase in neural activity compared to baseline was seen during 1s following cue onset (Figure 4D). Both delivery of a sugar pellet and administration of a foot shock resulted in a clear increase in neural activity in MC4R neurons (Figure 4C). Upon inspection of the results, we noted that the increase in neural activity during the pellet trials was related to retrieval/consumption of the pellet rather than to the delivery of it. Since the mice consumed the pellet at different timepoints following pellet delivery, while the shock is delivered at a fixed timepoint (Figure S5), we quantified the relative increase in neural activity within 2s surrounding pellet consumption and 2s following foot shock. This analysis revealed that both pellet consumption and foot shock administration induced robust calcium transients (pellet: t_5 = 8.50, $p < 0.001$; shock: t_5 = 16.75, $p < 0.001$). Moreover, transients in response to both events were of similar magnitude (t_5 = 0.41, ns; Figure 4E).

Dopamine is released in the LSS during sugar pellet consumption

Since dopamine is released in response to aversive stimuli, we tested the dopamine response in the LSS during the consumption of sugar pellets. Food-deprived mice were exposed to the same rewarding Pavlovian conditioning paradigm as described above. Dopamine release was measured in the LSS using a dLight1.2 sensor and fiber photometry. Dopamine release was evident in the LSS when the mice consumed the pellet, but no response was observed to the onset of the predictive tone (Figure 4F and Video S2). We could not see any reward prediction error encoded by dopamine release in the LSS, since unpredicted and predicted pellets generated equal responses, and the omission of a predicted pellet did not affect the dopamine release in any direction (Figures S4C and S4D). To compare the magnitudes of dopamine transients in sugar pellet and foot shock trials, trained mice were tested in a session consisting of 10 pellet deliveries followed by 10 foot shocks paired with cue lights. As seen in the previous fear-conditioning experiment, a robust dopamine release occurred in response to both the onset of a shock-predicting cue onset and foot shock delivery (Figure 4F). Comparison of the peak dopamine following cue onset showed a dopamine response to the light cue predicting a foot shock (t_4 = 4.86, p = 0.009), while no augmented dopamine activity was observed following onset of the tone cue predicting a sugar pellet (t_4 = 0.08, ns; Figure 4G). Further comparison of the peak dopamine signal surrounding pellet consumption and foot shock delivery (Figure 4H) revealed that dopamine transients induced by both events are significantly different from baseline activity (pellet: t_4 = 5.04, p = 0.007; shock: t_4 = 3.19, p = 0.03) and that the sugar pellet-induced dopamine release was larger than the foot shock-induced release t_4 = 3.69, p = 0.02). Notably, during the behavioral sessions, we observed that dopamine was released in response to both the onset and offset of the house light in the operant chamber, suggesting that dopamine is released in the LSS in response to salient stimuli (Figures S4E and S4F).

Activation of MC4R-LSS neurons is rewarding and increases locomotion

Since the striatum is highly involved in affective behaviors as well as motor initiation and given that the MC4R-LSS neurons are activated by both rewarding and aversive stimuli, we next investigated the valence and locomotor effect of optogenetic activation of these neurons (Figures 5A–5C). We found that optogenetic activation of MC4R-LSS neurons was reinforcing in an intracranial self-stimulation task, where ChR2-expressing mice, but not EYFP-expressing controls, were highly motivated to selectively nose-poke for unilateral light stimulation (F_{Opsin} (1, 14) = 18.96, $p < 0.001$; $F_{TimexOpsin}$ (2, 28) = 7.48, $p < 0.01$; Figure 5D), showing little to no interest for the inactive port (F_{Pokes} (1, 16) = 25.94, $p < 0.001$; $F_{TimexPokes}$ (2, 32) = 9.88, $p < 0.001$; Figure S6). The same ChR2-expressing mice exhibited a preference for the light-paired chamber in a real-time place preference paradigm, whereas the control group was indifferent to light stimulation (F_{Opsin} (1, 14) = 9.36, $p < 0.01$; $F_{TimexOpsin}$ (3, 42) = 4.08, p = 0.01; Figure 5E). We next tested exploratory behavior in an open field box. Activation of MC4R-LSS neurons for 5 min caused a robust increase in locomotion (Figure 5F), which ceased shortly after activation was stopped (F_{Opsin} (1, 14) = 4.19, p = 0.06; $F_{TimexOpsin}$ (2, 28) = 4.68, p = 0.02). Next, we investigated whether the rewarding and reinforcing effect of activating MC4R-neurons was specific to the LSS or if optogenetic activation in other parts of the striatum would generate similar results. Activation of MC4R-expressing neurons in the NAcC produced similar behavioral effects (Figures S7A–S7C) but no rewarding or reinforcing effects were observed by activating MC4R-neurons in the medial NAc shell (Figures S7D and S7E) or the dorsal striatum (Figures S7F and S7G). To assess whether MC4R-LSS neurons are necessary for voluntary locomotion, food intake, and energy homeostasis, we tested the impact of ablation of these neurons on locomotor behavior in an open field, voluntary wheel-running, food intake, and body weight. Ablation of the MC4R-LSS neurons with Caspase 3 did not result in a decrease in locomotion or wheel-running behavior, nor did it affect food intake or body weight (Figure S8). These results suggest that the MC4R-LSS neurons are part of the reward system and are involved in motor control, but that they are not necessary for voluntary movement, wheel-running behavior, or food intake.

Activation of MC4R-LSS neurons increases local dopamine release in the LSS *in vivo*

D1-neurons in the lateral NAc have been shown to increase dopaminergic cell firing via disinhibition in the lateral ventral tegmental area.[16] Using a dual optogenetic approach, we co-injected the constitutive dLight1.2 sensor and the cre-dependent, red-shifted opsin rsChrmine (or an mScarlet control virus) into the LSS of MC4R-cre mice. This allowed us to simultaneously measure dopamine release and manipulate MC4R-LSS-neuronal activity with blue and red light, respectively, through a chronically implanted fiber. Optogenetic activation of

(H) Maximal dF/F during 2s surrounding pellet consumption and 2s following the onset of the foot shock minus respective peak signal during 2s pre-cue baseline. Dopamine is released in response to both pellet consumption and foot shock. Pellet consumption-evoked dopamine release is higher than foot shock-evoked dopamine release. #$p < 0.05$, paired t-test comparing pellet vs. shock trials; *$p < 0.05$; **$p < 0.01$; ***$p < 0.001$, one-sample t-tests compared to a value of 0.

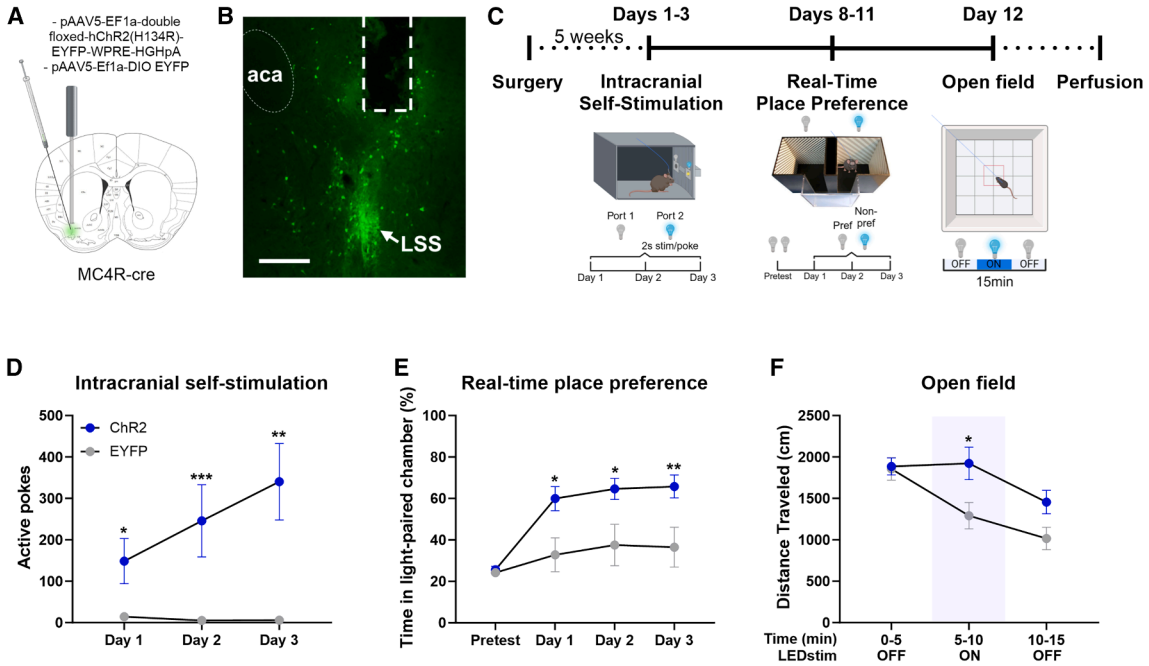

Figure 5. Optogenetic activation of MC4R-LSS neurons is rewarding and increases locomotion

(A) Experimental design for photoexcitation of MC4R-expressing neurons in the lateral stripe of the striatum (LSS).

(B) Representative image of a coronal striatal slice expressing ChR2 in MC4R-LSS neurons. Fiber tract and anterior commissure (aca) marked with dashed lines. LSS pointed out with an arrow. Scale bar 200 μm.

(C) Timeline of experiments.

(D) Mice learn to self-stimulate for unilateral activation of MC4R-LSS neurons in an optogenetic intracranial self-stimulation paradigm (n = 9 ChR2, n = 7 EYFP, repeated-measures ANOVA followed by Sidak's multiple comparisons test, ChR2 vs. EYFP).

(E) The same mice with ChR2 expression in MC4R-LSS neurons prefer a chamber paired with light stimulation, contrary to DIO-EYFP controls (n = 9 ChR2, n = 7 EYFP, repeated-measures ANOVA followed by Sidak's multiple comparisons test, ChR2 vs. EYFP).

(F) Open field locomotion before, during and after 5 min pulsed unilateral optogenetic stimulation of MC4R-LSS neurons. Data are shown per 5-min time bins (n = 9 ChR2, n = 7 EYFP, repeated-measures ANOVA followed by Sidak's multiple comparisons test, ChR2 vs. EYFP). All data are expressed as mean ± SEM. *p < 0.05; **p < 0.01; ***p < 0.001.

MC4R-LSS neurons led to a robust and dose-dependent increase in dopamine release in the LSS. The magnitude and duration of this dopamine response scaled with the light intensity (F_{Opsin} (1, 9) = 3.82, p = 0.08; $F_{TimexOpsin}$ (4, 36) = 3.45, p = 0.02) and stimulation duration (F_{Opsin} (1, 9) = 6.25, p = 0.03; $F_{TimexOpsin}$ (4, 36) = 7.35, p < 0.001), respectively. No effect on dopamine release was seen in the mScarlet control group except for a mild response to very high light powers in some mice (Figures 6A–6F). To test whether this dopamine release is mediated by a local circuit in the striatum, we conducted an *ex vivo* dual optogenetic experiment using striatal coronal slices. First, we validated that MC4R-LSS neurons could be activated in the setup by co-injecting viral vectors encoding cre-dependent GCaMP8m and rsChrmine in the LSS of one hemisphere and GCaMP8m and an mScarlet as a control in the other hemisphere of MC4R-cre mice. Stimulation of rsChrmine with red light induced robust and repeatable increases in GCaMP8m signal while no increase in GCaMP8m signal could be measured from the mScarlet control slices, indicating that MC4R-LSS neurons can be activated by red-shifted optogenetics in a coronal slice (Figure 6G). Further, coronal slices from MC4R-cre mice injected with constitutive dLight1.2 and cre-dependent rsChrmine in the LSS of one hemisphere and a dLight1.2 and an mScarlet control in the other were tested. While spontaneous dopamine releases could be measured in the slice, no dopamine release was observed in response to the activation of MC4R-LSS neurons, suggesting that the feedback loop is not mediated by a local striatal circuit (Figures 6H and S9).

DISCUSSION

Here, we present a functional characterization of MC4R-expressing neurons in the LSS. Our findings demonstrate that these neurons are activated by both rewarding and aversive stimuli, while the activation of this population is rewarding and reinforcing. In addition, we measured dopamine and glutamate release in the LSS during the same behavioral paradigms to compare neural activity with afferent neurotransmitter release, indicating that glutamate is the fast driver of MC4R-LSS neuronal activity. Our results also show a positive feedback loop from striatal medium spiny neurons to dopamine release within the same area.

Lately, multiple scRNA-seq papers have highlighted the heterogenicity among striatal medium spiny neurons and identified

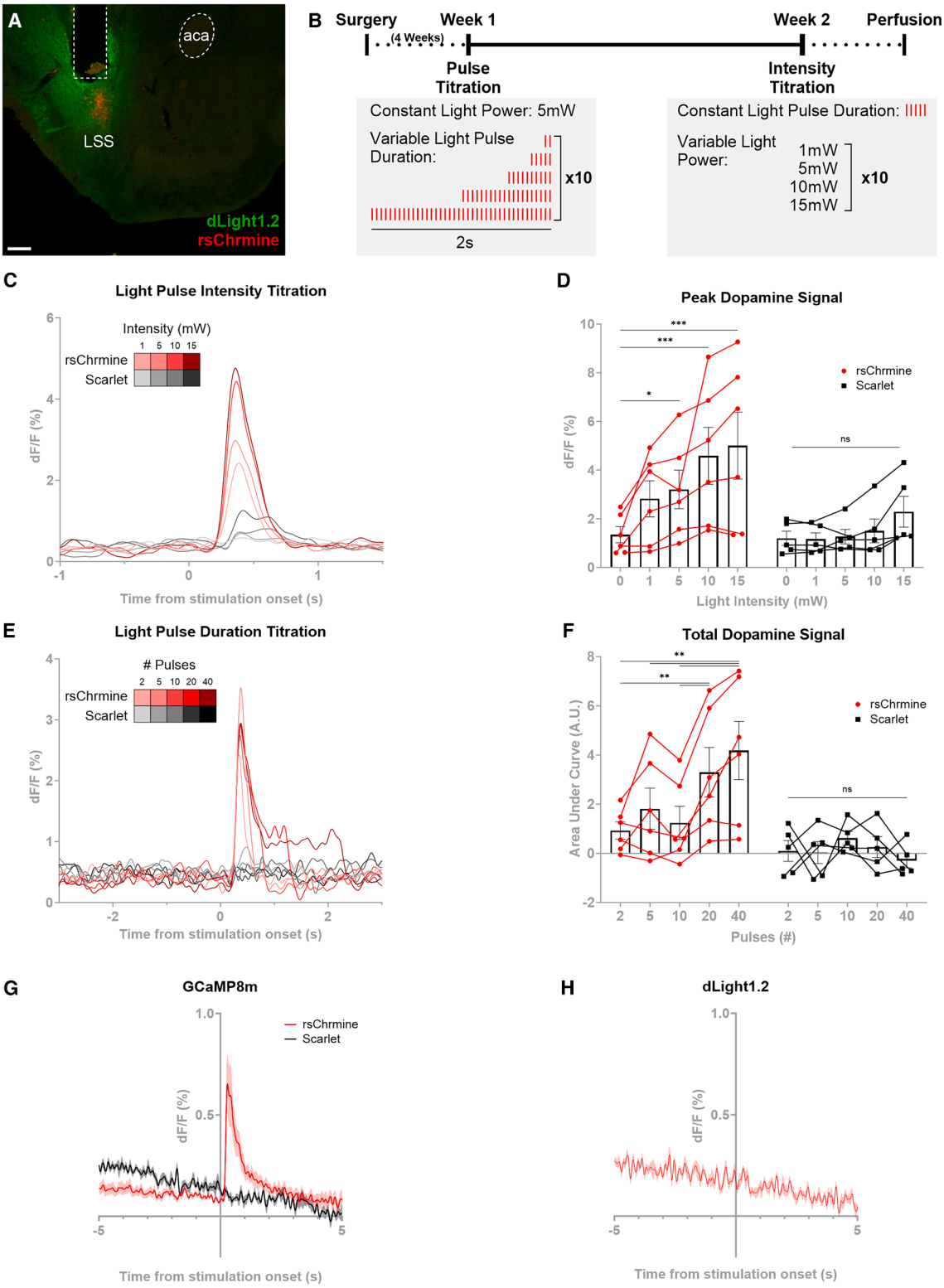

Figure 6. Activation of MC4R-LSS neurons causes a dose-dependent dopamine release in the lateral stripe of the striatum (LSS)

(A) Representative image of a coronal striatal slice expressing constitutive dLight1.2 (green) and rsChrmine-mScarlet (red) in MC4R-LSS neurons. Fiber tract and anterior commissure (aca) marked with dashed lines. Scale bar 200 μm.

(B) Timeline of dual optogenetics and fiber photometry experiment and trials.

(legend continued on next page)

atypical D1-neurons. One subpopulation of atypical D1-neurons is enriched in the LSS and expresses high levels of Tshz1 and FOXP2.[10–13] We found that the LSS is enriched in MC4R-expressing neurons and that they express D1-receptor and FOXP2, indicating that most MC4R-LSS neurons are atypical D1-neurons. Consequently, the MC4R-cre mouse line is an attractive tool to selectively target atypical D1-neurons of the LSS. Whereas the MC4R-LSS neurons were atypical at the transcriptional level, our tracing studies show that they share projection patterns with typical D1-neurons. Further, our optogenetic findings indicate that their behavioral function is similar to that of typical D1 neurons in that activation is rewarding and induces locomotion.[17–19] This contrasts the previous finding that activation of Tshz1-expressing cells (another marker of atypical D1-neurons) in the striosomes in the dorsal striatum was aversive.[20] The fact that activation of MC4R-neurons in the NAcC was also rewarding could indicate that the same neuronal type found in the LSS is present in the entire ventrolateral striatum or that there are two or more distinct populations of MC4R-expressing neurons with ability to induce reward.

We found that MC4R-LSS neurons were activated by both aversive and rewarding stimuli, suggesting that they detect salient events independent of valence. Although the MC4R-LSS neurons were activated also by aversive stimuli, their optogenetic activation was strongly rewarding. This might suggest that these neurons could, under certain circumstances, assign positive value to salient stimuli. Alternatively, there might be several sub-populations of MC4R-LSS neurons activated by different stimuli to induce distinct affects. The counterintuitive feature of being activated by aversive signals while mediating reward might relate to the finding that mice lacking MC4Rs develop place preference to both chambers paired with aversive and with rewarding stimuli, a phenotype that could be rescued by MC4R re-expression in D1 neurons in the striatum.[8] It is possible that the MC4R-neurons in the striatum are overactive or in another way given excessive weight in the valence assigning process in mice lacking MC4Rs. This would be in line with a study showing long-term depression of striatal D1 neurons after alpha-MSH stimulation.[7] However, it is unclear if the lack of MC4Rs affects the excitability of MC4R-LSS neurons. It is also unclear if, and in such case how, the MC4Rs in the LSS are activated in the context of aversion. MC4R-expression is found in many brain areas spared from hypothalamic POMC-neurons afferents,[21] and here we show that this is also the case for the LSS. It is possible that MC4R in the LSS can be activated by volume transmission of alpha-MSH or circulating Lipocalin 2 – which has been shown to be an MC4R-agonist.[22] Since the MC4R has a high constitutive activity,[23] it is possible that inverse agonists like agouti-related peptide could affect neural activity without the presence of an agonist. Alternatively, other, yet unidentified ligands could be the main effector of MC4R in the LSS, or the MC4R expression could lack physiological function.

In this study, we describe neural activity of MC4R-LSS neurons and dopamine release in the LSS during two different Pavlovian conditioning paradigms, one aversive and one rewarding. While foot shocks and pellet consumption triggered both neural activity peaks and dopamine release, there were several discrepancies between the two measurements. Dopamine was released in response to cues predicting aversive stimuli, while the MC4R-neurons did not show overt activity in response to conditioned stimuli. In the rewarding Pavlovian conditioning paradigm, we did not observe any dopamine response to the conditioned tone, despite extensive training, while dopamine response to cues predicting aversive outcomes was developed rapidly. This might be explained by the more salient and time-locked features of the foot shock in the fear conditioning compared to the pellet drop, where the animal can collect the pellet at any time after delivery. Alternatively, dopamine release in the LSS is more responsive to aversion prediction than to reward prediction. This would be surprising, however, since the dopamine release in response to reward consumption was higher than in response to the aversive foot shock.

Dopamine release in the striatum has been described as a saliency signal.[24–26] In line with this finding, we found that stimuli with seemingly limited value, such as the house light of the operant chamber turning on or off, caused robust dopamine release in the LSS. However, although the initial dopamine response to an aversive foot shock was positive, the dopamine signal was lower than baseline at the end of the shock. This could indicate a mixed response from dopaminergic terminals, where one population increases the firing due to salience and the other is inhibited by negative value. The dopamine release in response to foot shock was not LSS-specific, since the same pattern could be seen in the NAcC. These

(C) Traces from light intensity titration show a positive dose-response relationship between red light optogenetic activation of MC4R-LSS neurons expressing rsChrmine and dopamine release in the LSS.

(D) Same data as in (C) displayed as maximal dF/F within 1s following stimulation showing a significant dose-response relationship between peak dopamine release and light intensity in the rsChrmine group but not in the mScarlet controls (repeated-measures ANOVA followed by Sidak's multiple comparisons test. Data for 0 mW stimulation analyzed from 1s before stimulation start).

(E) Increased stimulation duration of MC4R-LSS neurons increases the duration of elevated dopamine in the LSS.

(F) Same data as in (E) expressed as area under the curve during 3s after stimulation start minus area under the curve 3s before stimulation start showing a significant dose-response relationship between total dopamine release and light pulse duration in the rsChrmine (red) group but not in the mScarlet (black) controls ($n = 6$ rsChrmine, $n = 5$ Scarlet controls, each datapoint in (D and F) represents a mean from 10 repeated trials.; repeated-measures ANOVA followed by Sidak's multiple comparisons test).

(G) MC4R-LSS neurons in a coronal slice can be activated by the red-shifted opsin rsChrmine. Traces showing increased GCaMP8m signal from MC4R-neurons during optogenetic stimulation while the GCaMP8m signal from control slices is unaffected ($n = 16$ rsChrmine slices from 4 animals, $n = 6$ control slices from 2 animals).

(H) Same as in (G) but for dLight1.2 measurements. No dopamine release was seen in response to optogenetic stimulation of MC4R-LSS neurons, indicating that there is no local feedback-loop ($n = 7$ slices from 3 animals). $^{*}p < 0.05$; $^{**}p < 0.01$; $^{***}p < 0.001$. Data expressed as mean ± SEM except for (C and E) where data is expressed as mean.

findings contrast previous studies suggesting that aversive stimuli lead to a decrease in striatal dopamine in all subregions.[27] Possibly, this discrepancy could be due to the use of different dopamine measurement techniques (fast-scan cyclic voltammetry versus photometry) and different aversive stimuli, where the foot shock we delivered is likely to be more salient than the white noise used in the aforementioned study. Since the by-far largest dopamine responses recorded in our study were in response to consumption of rewarding sugar pellets, dopamine could have a dual role of saliency signaling and reward signaling in the LSS and NAcC, possibly via heterogeneous dopaminergic neural populations.[15]

Dopamine and the striatum are well known for their involvement in motor functions. Here, we found a clear correlation between body movements of the animal, including those not leading to locomotion, and the activity of MC4R-LSS neurons. Moreover, artificial activation of these neurons increased locomotion. This strongly suggests that the neurons are involved in movement control and highlights the importance to consider the impact of all body movements when studying the striatum. The fact that ablation of the MC4R-LSS neurons did not affect locomotion could be explained by the small numbers of neurons affected, compared to the whole striatum, as the movement correlation is not LSS- or MC4R-specific. Whereas MC4R-LSS-neural activity was correlated to movement on a short timescale, we show that the dopamine release in the LSS was not. Even though dopamine has been shown to drive neural activity with sub-second resolution *ex vivo*,[28] this was not the case in our *in vivo* experiments. Rather, the discrepancies in neural activity and dopamine release during Pavlovian conditioning experiments and the observation that the administration of a D1-antagonist did not attenuate the foot shock–induced neural activity strongly implies that the fast, neural activity driving input to striatal neurons is not dopamine. Likely, the main driver of acute changes in MC4R-LSS-neuronal activity is glutamatergic cortico-striatal inputs, with dopamine acting as a slow modulator, since glutamate is released in the LSS in a pattern similar to the activity of MC4R-LSS neurons. While dopamine is not the primary acute driver of activity of the MC4R-LSS neurons, we instead show a causal relationship between activity of MC4R-LSS neurons and dopamine release in the LSS. This is likely mediated via disinhibition in the midbrain, since there are strong projections from MC4R-LSS neurons to the substantia nigra pars reticulata. Moreover, no dopamine release was seen when MC4R-LSS neurons were activated in a coronal slice, where these projections were severed. Our finding that stimulating MC4R-LSS neurons leads to dopamine release in the stimulated area *in vivo* complements a previous electrophysiological study showing that D1-neurons in the ventrolateral striatum can increase the activity of midbrain dopaminergic neurons through disinhibition.[16]

In conclusion, MC4R-LSS neurons are primarily atypical D1-neurons that are activated by both aversive and rewarding stimuli, while their activation is rewarding and induces locomotion. The ability of MC4R-LSS neurons to detect salient stimuli, regardless of valence, and to induce positive affect might play a crucial role in assigning value to salient stimuli under certain conditions.

Limitations of the study

Even though we used a MC4R-cre transgenic mouse line and stereotactic surgeries to specifically target MC4R-LSS neurons, both optogenetic and fiber photometry techniques have inherent limitations in spatial specificity. While the placement of the optical fibers ensured that the majority of the targeted neurons were located in the LSS, the size of the fibers relative to the small size of the LSS precludes us from excluding the possibility that MC4R-neurons adjacent to the LSS contributed to the behavioral effects or neural responses we observed using these techniques. Our optical methods also lack cellular resolution. Thus, it could be that we missed more subtle divisions of MC4R-LSS neurons into subclusters with different functional roles. A second limitation of our study is the apparent lack of behavioral effects of chronic ablation of MC4R-LSS neurons in the caspase experiment. Indeed, this manipulation neither affected locomotion in the open field test or the wheel running experiment, nor did it alter food intake. On the other hand, we observed clear hyperlocomotion upon optogenetic activation of this neuronal cluster. One interpretation of these contrasting findings could be that although the activity MC4R-LSS neurons can modulate motor behavior, it is not necessary for such behavior. Alternatively, compensatory mechanisms following the chronic ablation of these neurons may have occluded any behavioral effects. Future studies could use acute inhibition of these neurons with opto- or chemogenetic techniques and/or other behavioral readouts to better understand the physiological functions of MC4R-LSS neurons. Finally, it should be noted that although we established a role for MC4R-LSS neurons in affect regulation and motor control, the functional role of MC4R signaling in these neurons was not addressed in this study. The identification of such a role might be complicated by the sparse POMC innervation of the LSS.

RESOURCE AVAILABILITY

Lead contact

Further information and requests for resources and reagents should be directed to and will be fulfilled by the lead contact, David Engblom (david.engblom@liu.se).

Materials availability

This study did not generate new unique reagents.

Data and code availability

- Data: All data reported in this paper will be shared by the lead contact upon request.
- Code: All original code used for the fiber photometry analyses has been deposited at Zenodo (MATLAB scripts to perform cross-correlation analysis) or Github (general fiber photometry data analysis pipeline) and is publicly available as of the date of publication. DOIs are listed in the key resources table.
- Additional information: Any additional information required to reanalyze the data reported in this paper is available from the lead contact upon request.

ACKNOWLEDGMENTS

We thank the staff at the animal facility for technical assistance regarding animal breeding and care. We thank Maria Ntzouni and Vesa Loitto from histology and imaging facilities at Linköping Microscopy Unit for technical assistance.

We also thank Larri Mohell Malinen, Johannes Sjölin, Vilma Odland, and Sertan Arkan for their technical assistance, Ilona Szczot for her help with the development of the fiber photometry analysis software, Michele Petrella for his help with the *ex vivo* slice preparations, and Anders Blomqvist for fruitful discussions on the design and results. Finally, we thank the Technical Platform for Optogenetics and Optical Imaging from the Center for Systems Neurobiology at Linköping University, as well as Markus Heilig, for their role in establishing the local infrastructure for optogenetics and fiber photometry experiments. Part of the figures were created with biorender.com. This study was supported by the Knut and Alice Wallenberg foundation, the Swedish Research Council (2022-00952 and 2022–06568), the Swedish Brain Foundation (FO2022-0114 and 2024-0263), Stiftelsen för Parkinsonforskning at Linköping University and Lions forskningsfond mot folksjukdomar.

AUTHOR CONTRIBUTIONS

Conceptualization, D.E., G.P.L., J.S., and J.W.; methodology, D.E., G.P.L., J. S., and J.W.; software programming, J.W.; validation, G.P.L. and J.S.; formal analysis, G.P.L. and J.S.; investigation, G.P.L., J.S., and M.N.; resources, D.E.; data curation, D.E., G.P.L., J.S., and J.W.; writing – original draft, G.P.L. and J. S.; writing – review and editing, D.E., G.P.L., J.S., and J.W.; visualization, G.P. L. and J.S.; supervision, D.E. and J.W.; project administration, D.E.; funding acquisition, D.E. and G.P.L.

DECLARATION OF INTERESTS

The authors declare no competing interests.

STAR★METHODS

Detailed methods are provided in the online version of this paper and include the following:

- KEY RESOURCES TABLE
- EXPERIMENTAL MODEL AND STUDY PARTICIPANT DETAILS
  - Animals
- METHOD DETAILS
  - Viral constructs
  - Stereotactic injections and optic fiber implantation
  - Fiber photometry
  - Behavioral paradigms
- QUANTIFICATION AND STATISTICAL ANALYSIS
  - Statistics

SUPPLEMENTAL INFORMATION

Supplemental information can be found online at https://doi.org/10.1016/j.isci.2025.112456.

Received: July 3, 2024
Revised: October 4, 2024
Accepted: April 11, 2025
Published: April 16, 2025

REFERENCES

1. Tye, K.M., Mirzabekov, J.J., Warden, M.R., Ferenczi, E.A., Tsai, H.C., Finkelstein, J., Kim, S.Y., Adhikari, A., Thompson, K.R., Andalman, A.S., et al. (2013). Dopamine neurons modulate neural encoding and expression of depression-related behaviour. Nature *493*, 537–541. https://doi.org/10.1038/nature11740.
2. de Jong, J.W., Afjei, S.A., Pollak Dorocic, I., Peck, J.R., Liu, C., Kim, C.K., Tian, L., Deisseroth, K., and Lammel, S. (2019). A Neural Circuit Mechanism for Encoding Aversive Stimuli in the Mesolimbic Dopamine System. Neuron *101*, 133–151.e7. https://doi.org/10.1016/j.neuron.2018.11.005.
3. Bromberg-Martin, E.S., Matsumoto, M., and Hikosaka, O. (2010). Dopamine in Motivational Control: Rewarding, Aversive, and Alerting. Neuron *68*, 815–834. https://doi.org/10.1016/j.neuron.2010.11.022.
4. Klawonn, A.M., and Malenka, R.C. (2018). Nucleus accumbens modulation in reward and aversion. Cold Spring Harb. Symp. Quant. Biol. *83*, 119–129. https://doi.org/10.1101/sqb.2018.83.037457.
5. Belujon, P., and Grace, A.A. (2017). Dopamine system dysregulation in major depressive disorders. Int. J. Neuropsychopharmacol. *20*, 1036–1046. https://doi.org/10.1093/ijnp/pyx056.
6. Pandit, R., Van Der Zwaal, E.M., Luijendijk, M.C.M., Brans, M.A.D., Van Rozen, A.J., Oude Ophuis, R.J.A., Vanderschuren, L.J.M.J., Adan, R.A. H., and la Fleur, S.E. (2015). Central melanocortins regulate the motivation for sucrose reward. PLoS One *10*, e0121768. https://doi.org/10.1371/journal.pone.0121768.
7. Lim, B.K., Huang, K.W., Grueter, B.A., Rothwell, P.E., and Malenka, R.C. (2012). Anhedonia requires MC4R-mediated synaptic adaptations in nucleus accumbens. Nature *487*, 183–189. https://doi.org/10.1038/nature11160.
8. Klawonn, A.M., Fritz, M., Nilsson, A., Bonaventura, J., Shionoya, K., Mirrasekhian, E., Karlsson, U., Jaarola, M., Granseth, B., Blomqvist, A., et al. (2018). Motivational valence is determined by striatal melanocortin 4 receptors. J. Clin. Investig. *128*, 3160–3170. https://doi.org/10.1172/JCI97854.
9. Liu, H., Kishi, T., Roseberry, A.G., Cai, X., Lee, C.E., Montez, J.M., Friedman, J.M., and Elmquist, J.K. (2003). Transgenic mice expressing green fluorescent protein under the control of the melanocortin-4 receptor promoter. J. Neurosci. *23*, 7143–7154. https://doi.org/10.1523/jneurosci.23-18-07143.2003.
10. Gokce, O., Stanley, G.M., Treutlein, B., Neff, N.F., Camp, J.G., Malenka, R. C., Rothwell, P.E., Fuccillo, M.V., Südhof, T.C., and Quake, S.R. (2016). Cellular Taxonomy of the Mouse Striatum as Revealed by Single-Cell RNA-Seq. Cell Rep. *16*, 1126–1137. https://doi.org/10.1016/J.CELREP.2016.06.059.
11. Saunders, A., Macosko, E.Z., Wysoker, A., Goldman, M., Krienen, F.M., de Rivera, H., Bien, E., Baum, M., Bortolin, L., Wang, S., et al. (2018). Molecular Diversity and Specializations among the Cells of the Adult Mouse Brain. Cell *174*, 1015–1030.e16. https://doi.org/10.1016/j.cell.2018.07.028.
12. Chen, R., Blosser, T.R., Djekidel, M.N., Hao, J., Bhattacherjee, A., Chen, W., Tuesta, L.M., Zhuang, X., and Zhang, Y. (2021). Decoding molecular and cellular heterogeneity of mouse nucleus accumbens. Nat. Neurosci. *24*, 1757–1771. https://doi.org/10.1038/s41593-021-00938-x.
13. Stanley, G., Gokce, O., Malenka, R.C., Südhof, T.C., and Quake, S.R. (2020). Continuous and Discrete Neuron Types of the Adult Murine Striatum. Neuron *105*, 688–699.e8. https://doi.org/10.1016/j.neuron.2019.11.004.
14. Hunnicutt, B.J., Jongbloets, B.C., Birdsong, W.T., Gertz, K.J., Zhong, H., and Mao, T. (2016). A comprehensive excitatory input map of the striatum reveals novel functional organization. Elife *5*, e19103. https://doi.org/10.7554/ELIFE.19103.
15. De Jong, J.W., Fraser, K.M., and Lammel, S. (2022). Mesoaccumbal Dopamine Heterogeneity: What Do Dopamine Firing and Release Have to Do with It? Annu. Rev. Neurosci. *45*, 109–129. https://doi.org/10.1146/annurev-neuro-110920-011929.
16. Yang, H., de Jong, J.W., Tak, Y., Peck, J., Bateup, H.S., and Lammel, S. (2018). Nucleus Accumbens Subnuclei Regulate Motivated Behavior via Direct Inhibition and Disinhibition of VTA Dopamine Subpopulations. Neuron *97*, 434–449.e4. https://doi.org/10.1016/j.neuron.2017.12.022.
17. Cole, S.L., Robinson, M.J.F., and Berridge, K.C. (2018). Optogenetic self-stimulation in the nucleus accumbens: D1 reward versus D2 ambivalence. PLoS One *13*, e0207694. https://doi.org/10.1371/journal.pone.0207694.
18. Kravitz, A.V., Freeze, B.S., Parker, P.R.L., Kay, K., Thwin, M.T., Deisseroth, K., and Kreitzer, A.C. (2010). Regulation of parkinsonian motor

behaviors by optogenetic control of basal ganglia circuitry. Nature *466*, 622–626. https://doi.org/10.1038/NATURE09159.

19. Soares-Cunha, C., Coimbra, B., Sousa, N., and Rodrigues, A.J. (2016). Reappraising striatal D1- and D2-neurons in reward and aversion at Pergamon. Neurosci Biobehav Rev. *68*, 370–386. https://doi.org/10.1016/j.neubiorev.2016.05.021.
20. Xiao, X., Deng, H., Furlan, A., Yang, T., Zhang, X., Hwang, G.R., Tucciarone, J., Wu, P., He, M., Palaniswamy, R., et al. (2020). A Genetically Defined Compartmentalized Striatal Direct Pathway for Negative Reinforcement. Cell *183*, 211–227.e20. https://doi.org/10.1016/j.cell.2020.08.032.
21. Lima, L.B., Pedroso, J.A.B., Metzger, M., Gautron, L., and Donato, J. (2019). Relationship of α-MSH and AgRP axons to the perikarya of melanocortin-4 receptor neurons. Brain Res. *1717*, 136–146. https://doi.org/10.1016/j.brainres.2019.04.021.
22. Mosialou, I., Shikhel, S., Liu, J.M., Maurizi, A., Luo, N., He, Z., Huang, Y., Zong, H., Friedman, R.A., Barasch, J., et al. (2017). MC4R-dependent suppression of appetite by bone-derived lipocalin 2. Nature *543*, 385–390. https://doi.org/10.1038/nature21697.
23. Kleinau, G., Heyder, N.A., Tao, Y.X., and Scheerer, P. (2020). Structural Complexity and Plasticity of Signaling Regulation at the Melanocortin-4 Receptor at Multidisciplinary Digital (Publishing Institute). https://doi.org/10.3390/ijms21165728.
24. Kutlu, M.G., Zachry, J.E., Melugin, P.R., Cajigas, S.A., Chevee, M.F., Kelly, S.J., Kutlu, B., Tian, L., Siciliano, C.A., and Calipari, E.S. (2021). Dopamine release in the nucleus accumbens core signals perceived saliency. Curr. Biol. *31*, 4748–4761.e8. https://doi.org/10.1016/j.cub.2021.08.052.
25. Kutlu, M.G., Tat, J., Christensen, B.A., Zachry, J.E., and Calipari, E.S. (2023). Dopamine release at the time of a predicted aversive outcome causally controls the trajectory and expression of conditioned behavior. Cell Rep. *42*, 112948. https://doi.org/10.1016/J.CELREP.2023.112948.
26. Yawata, Y., Shikano, Y., Ogasawara, J., Makino, K., Kashima, T., Ihara, K., Yoshimoto, A., Morikawa, S., Yagishita, S., Tanaka, K.F., and Ikegaya, Y. (2023). Mesolimbic dopamine release precedes actively sought aversive stimuli in mice. Nat. Commun. *14*, 2433. https://doi.org/10.1038/s41467-023-38130-3.
27. van Elzelingen, W., Goedhoop, J., Warnaar, P., Denys, D., Arbab, T., and Willuhn, I. (2022). A unidirectional but not uniform striatal landscape of dopamine signaling for motivational stimuli. Proc. Natl. Acad. Sci. USA *119*, e2117270119. https://doi.org/10.1073/pnas.2117270119.
28. Lahiri, A.K., and Bevan, M.D. (2020). Dopaminergic Transmission Rapidly and Persistently Enhances Excitability of D1 Receptor-Expressing Striatal Projection Neurons. Neuron *106*, 277–290.e6. https://doi.org/10.1016/j.neuron.2020.01.028.
29. Garfield, A.S., Li, C., Madara, J.C., Shah, B.P., Webber, E., Steger, J.S., Campbell, J.N., Gavrilova, O., Lee, C.E., Olson, D.P., et al. (2015). A neural basis for melanocortin-4 receptor-regulated appetite. Nat. Neurosci. *18*, 863–871. https://doi.org/10.1038/nn.4011.
30. Madisen, L., Zwingman, T.A., Sunkin, S.M., Oh, S.W., Zariwala, H.A., Gu, H., Ng, L.L., Palmiter, R.D., Hawrylycz, M.J., Jones, A.R., et al. (2010). A robust and high-throughput Cre reporting and characterization system for the whole mouse brain. Nat. Neurosci. *13*, 133–140. https://doi.org/10.1038/nn.2467.
31. Ade, K.K., Wan, Y., Chen, M., Gloss, B., and Calakos, N. (2011). An Improved BAC Transgenic Fluorescent Reporter Line for Sensitive and Specific Identification of Striatonigral Medium Spiny Neurons. Front. Syst. Neurosci. *5*, 32. https://doi.org/10.3389/FNSYS.2011.00032.
32. Balthasar, N., Coppari, R., McMinn, J., Liu, S.M., Lee, C.E., Tang, V., Kenny, C.D., McGovern, R.A., Chua, S.C., Elmquist, J.K., and Lowell, B. B. (2004). Leptin receptor signaling in POMC neurons is required for normal body weight homeostasis. Neuron *42*, 983–991. https://doi.org/10.1016/j.neuron.2004.06.004.
33. Barchiesi, R., Chanthongdee, K., Petrella, M., Xu, L., Söderholm, S., Domi, E., Augier, G., Coppola, A., Wiskerke, J., Szczot, I., et al. (2022). An epigenetic mechanism for over-consolidation of fear memories. Mol. Psychiatry *27*, 4893–4904. https://doi.org/10.1038/s41380-022-01758-6.
34. Lerner, T.N., Shilyansky, C., Davidson, T.J., Evans, K.E., Beier, K.T., Zalocusky, K.A., Crow, A.K., Malenka, R.C., Luo, L., Tomer, R., and Deisseroth, K. (2015). Intact-Brain Analyses Reveal Distinct Information Carried by SNc Dopamine Subcircuits. Cell *162*, 635–647. https://doi.org/10.1016/j.cell.2015.07.014.
35. Bruno, C.A., O'Brien, C., Bryant, S., Mejaes, J.I., Estrin, D.J., Pizzano, C., and Barker, D.J. (2021). pMAT: An Open-Source Software Suite for the Analysis of Fiber Photometry Data. Pharmacol. Biochem. Behav. *201*, 173093. https://doi.org/10.1016/J.PBB.2020.173093.

STAR★METHODS

KEY RESOURCES TABLE

REAGENT or RESOURCE	SOURCE	IDENTIFIER
Antibodies		
Rabbit anti-foxP2	Abcam	Cat# ab16046, RRID:AB_2107107
Rabbit anti-red fluorescent protein	MBL International	Cat# PM005, RRID:AB_591279
chicken anti-GFP	Abcam	Cat# ab13970, RRID:AB_300798
Donkey anti-Rabbit IgG (H + L) Highly Cross-Adsorbed Secondary Antibody, Alexa Fluor™ 488	Invitrogen	Cat# A21206, RRID:AB_2535792
Donkey anti-Rabbit IgG (H + L) Highly Cross-Adsorbed Secondary Antibody, Alexa Fluor™ 568	Invitrogen	Cat# A10042, RRID:AB_2534017
Goat anti-Chicken IgY (H + L) Secondary Antibody, Alexa Fluor™ 488	Invitrogen	Cat# A11039, RRID:AB_2534096
Bacterial and virus strains		
pAAV-EF1a-doublefloxed-hChR2(H134R)-EYFP-WPRE-HGHpA	Addgene	AddGene AAV5, 20298-AAV5
pAAV5-Ef1a-DIO-EYFP	Addgene	20298-AAV5
pAAV5-EF1a-double floxed-hChR2 (H134R)-mCherry-WPRE-HGHpA	Addgene	20297-AAV5
pAAV1-Ef1a-fDIO mCherry	Addgene	114471-AAV1
pAAV5-flex-taCasp3-TEVp	Addgene	45580-AAV5
pGP-AAV9-*syn*-FLEX-jGCaMP8m-WPRE	Addgene	162378-AAV9
pAAV5-hSyn-dlight1.2	Addgene	111068-AAV5
AAV9.CamKII.GCaMP6s.WPRE.SV40	Addgene	107790-AAV9
ssAAV-1-hSyn1-chI-dlox-SF_iGluSnFR (A184S)(rev)-dlox-WPRE-SV40p(A)	Zürich Viral Vector Facility	v357-1
pAAV8-Ef1a-DIO-rsChRmine-oScarlet-WPRE	Stanford Gene Vector and Virus Core (RRID:SCR_023250)	GVVC-AAV-215
pAAV8-Ef1a-DIO-mScarlet-WPRE	Stanford Gene Vector and Virus Core (RRID:SCR_023250)	GVVC-AAV-187
Chemicals, peptides, and recombinant proteins		
Buprenorphine	Orion Pharma	N02AE01
Carprofen	Pfizer	141–053
Isoflurane	Attane Vet	Vnr 170579
Super-bond C&B	Sun Medical co.	K058E
Ortho-Jet black powder	Lang Dental Manufacturing Co.	N/A
Ortho-Jet black liquid	Lang Dental Manufacturing Co.	N/A
SCH23390 hydrochloride	Tocris	Cat# 0925
4% Paraformaldehide	Solveco	Vnr 754122
Isopentane		
Critical commercial assays		
RNAscope Multiplex Fluorescent Reagent Kit v2	Advanced Cell Diagnostics	Cat. No. 323100
mc4r probe	Advanced Cell Diagnostics	Cat No. 319181
Experimental models: Organisms/strains		
Mouse: Mc4rtm3.1(cre)Lowl/J	The Jackson Laboratory	Cat# 030759, RRID:IMSR_JAX:030759
Mouse: B6.Cg-Gt(ROSA)26Sortm9(CAG-tdTomato)Hze/J	The Jackson Laboratory	Cat# 007909, RRID:IMSR_JAX:007909

(*Continued on next page*)

Continued

REAGENT or RESOURCE	SOURCE	IDENTIFIER
Mouse: B6.Cg-Tg(Mc4r-MAPT/Sapphire) 21Rck/J	The Jackson Laboratory	Cat# 008323, RRID:IMSR_JAX:008323
Mouse: B6.Cg-Tg(Drd1a-tdTomato) 6Calak/J	The Jackson Laboratory	Cat# 016204, RRID:IMSR_JAX:016204
Mouse: Tg(Pomc1-cre)16Lowl/J	The Jackson Laboratory	Cat# 005965, RRID:IMSR_JAX:005965
Mouse: 129S6.FVB(B6)-Tg(Drd1a-cre) AGsc/KndlJ	The Jackson Laboratory	Cat# 028298, RRID:IMSR_JAX:028298
Mouse: MC4R-tdTomato	This paper	N/A
Mouse: Drd1-tdTomato-MC4R-eGFP	This paper	N/A
Software and algorithms		
EthoVision XT 17	Noldus	https://www.noldus.com/ethovision-xt
GraphPad Prism v10.0.2	GraphPad Software	https://www.graphpad.com/
ImageJ 1.52i	NIH	https://imagej.net/ij/download.html
Synapse v98	Tucker-Davis Technologies	https://www.tdt.com/component/synapse-software/
Med-PC IV	Med Associates Inc.	Version 4.42, build 58
MATLAB	Mathworks	http://www.Mathworks.com
Python 3.7	Python	https://www.python.org
Anaconda 3	Anaconda software distribution	Vers. 2023.09
Fiber photometry analysis software	In-house	https://github.com/ilo21/fpExplorer https://doi.org/10.5281/zenodo.15024685
Other		
Dustless Precision Pellets, Sucrose	Bio-Serv	Cat# F07595
Animal Stereotaxic Instrument	Kopf	942-C
gastight Neuros syringe (33G)	Hamilton	65460–05
UMP3 micro-syringe injector	World Precision Instruments Inc	N/A
Micro4 controller	World Precision Instruments Inc	N/A
Optic fiber implants O.D. 5 mm, Fiber Core 200/250μm, NA 0.66	Doric Lenses Inc.	B280-2617-5.0
Optic fiber implants O.D. 5 mm, Fiber Core 400/430μm, NA 0.66	Doric Lenses Inc.	B280-4604-5
1x1 Fiber Optic Low Friction Rotary Joint	Prizmatix	N/A
Pigtailed 1x1 Fiber-optic Rotary Joint	Doric Lenses Inc.	FRJ_1x1_PT _400–0.57_1.5m_FCM_0.15m_CM3
LED source	Prizmatix	Optogenetics-LED-Blue & Optogenetics-LED-Orange-Red
Standard mouse operant conditioning chamber	Med Associates	ENV-307W
Spatial Place Preference Box (Panlab)	Harvard Apparatus	76–0278
Vertical wireless running wheels	Med Associates	ENV-044V+DIG-804
Real-time processor for fiber photometry	Tucker-Davis Technologies	RZ5P
5-ports fluorescence minicube with build-in photodetector	Doric Lenses Inc.	iFMC5-G2_IE(400–410)_E(460–490)_F (500–540)_O(580–680)__S
LED sources	Doric Lenses Inc.	CLED_405 & CLED_465
LED driver	Doric Lenses Inc.	LEDD_2
USB camera	ELP	ELP-USBFHD06H-BL100
Opal 570 tyramide	Akoya Biosciences	SKU FP1488001KT
Vibratome	Leica	VT1200S
Cryostat	Leica	CM1959
Freezing microtome	Leica	CM1325
Superfrost plus microscope slides	Thermo Scientific	J1800AMNZ

(*Continued on next page*)

Continued

REAGENT or RESOURCE	SOURCE	IDENTIFIER
Cover glass	VWR	Cat# 631-0146
ProLong Glass Antifade Mounting agent	Thermofisher	P36984
Confocal microscope	Carl Zeiss AG	LSM 700
Widefield microscope	Leica	DMi8

EXPERIMENTAL MODEL AND STUDY PARTICIPANT DETAILS

Animals

Experimental protocols were conducted according to international and national guidelines for animal research and were approved by the Research Animal Care and Use Committee in Linköping, Sweden (main study approval number: 13844-2020).

All experiments were done using mice aged between 8 and 20 weeks at the onset of experiments. Animals were kept in a pathogen-free facility on a regular 12-h light/dark cycle (lights off 07.00 p.m.) and a temperature of 22 ± 2°C in individually ventilated cages. All experiments were performed in the light phase. Food and water were provided *ad libitum*, unless otherwise stated. Mc4rtm3.1(cre) Lowl/J (Mc4r-cre, #030759), B6.Cg-Gt(ROSA)26Sortm9(CAG-tdTomato)Hze/J (Ai9, #007909), B6.Cg-Tg(Mc4r-MAPT/Sapphire) 21Rck/J (Mc4r-GFP, #008323), B6.Cg-Tg(Drd1a-tdTomato)6Calak/J (Drd1-tdTomato, #016204), 129S6.FVB(B6)-Tg(Drd1a-cre) AGsc/KndlJ (D1-cre, #028298) and Tg(Pomc1-cre)16Lowl/J (POMC-cre, #005965) lines have previously been described in the literature,[9,29–32] and were purchased from The Jackson Laboratory. MC4R-tdTomato animals were obtained by crossing Mc4-cre and Ai9 lines, and Drd1-tdTomato-MC4R-eGFP line was obtained by crossing Mc4r-GFP and Drd1-tdTomato. All mice used in this study had a C57BL/6 background, except for POMC-Cre (mixed FVB/N and C57BL/6J strains). Animals were assigned into different experimental groups balanced by sex and age, and single housed after surgeries. We did not observe any noticeable differences in the results between male and female mice. As a result, data obtained from both sexes were combined.

METHOD DETAILS

Viral constructs

The following viruses used in the current study were obtained from AddGene: pAAV5-EF1a-doublefloxed-hChR2(H134R)-EYFP-WPRE-HGHpA (20298-AAV5; ChR2), pAAV5-Ef1a-DIO-EYFP (27056-AAV5; EYFP), pAAV5-EF1a-double floxed-hChR2(H134R)-mCherry-WPRE-HGHpA (20297-AAV5; ChR2-mCherry), pAAV1-Ef1a-fDIO mCherry (114471-AAV1; mCherry), pAAV5-flex-taCasp3-TEVp (45580-AAV5; Casp3), pGP-AAV9-*syn*-FLEX-jGCaMP8m-WPRE (162378-AAV9; GCaMP8m), pAAV5-hSyn-dlight1.2 (111068-AAV5; dlight1.2) AAV9.CamKII.GCaMP6s.WPRE.SV40 (107790-AAV9; GCaMP6s). ssAAV-1-hSyn1-chI-dlox-SF_iGluSnFR(A184S)(rev)-dlox-WPRE-SV40p(A) (v357-1; SF_iGluSnFR) was obtained from the Zürich Viral Vector Facility. pAAV8-Ef1a-DIO-rsChRmine-oScarlet-WPRE (rsChRmine) and pAAV8-Ef1a-DIO-mScarlet-WPRE (mScarlet) were obtained from the Deisseroth Lab via the Stanford Gene Vector and Virus Core (RRID:SCR_023250). All vector titers ranged from $8.4x10^{12}$ to $2.3x10^{13}$ viral particles/ml.

Stereotactic injections and optic fiber implantation

For all stereotactic surgeries, mice first received a subcutaneous injection of buprenorphine (0.01 mg/kg; Vetergesic vet; Orion Pharma) as an analgesic 30 min prior to intervention. Subsequently, mice were anesthetized with 3% isoflurane, placed in a stereotaxic apparatus (David Kopf Instruments), and maintained at a constant isoflurane level of 1.0–1.5% throughout the surgical process. Adeno-associated virus (AAV) vectors were unilaterally injected at a rate of 100 nL/min using a gastight Hamilton Neuros syringe (33G), an UMP3 micro-syringe injector and a Micro4 controller (World Precision Instruments Inc.). All injections (300 nL) were performed in the LSS using the following coordinates from bregma: Anterior/posterior [AP]: 1.1; medial/lateral [ML]: ±2.0; dorsal/ventral [DV]: −4.7 for fiber photometry experiments, and [DV]: −4.9 for optogenetic experiments. For projection mapping analysis, 100 nL of pAAV5-Ef1a-DIO EYFP was injected in the LSS of MC4r-cre mice using the aforementioned coordinates, or in the arcuate nucleus (ARC) of POMC-cre animals, using the coordinates AP: −1,5; ML: ±0,5; DV: −5,8. To induce neuronal ablation, 300 nL of a mixture of pAAV5-flex-taCasp3-TEVp with pAAV5-Ef1a-DIO-EYFP (9:1) was bilaterally injected into the LSS of MC4r-cre mice or their wild type littermates (control group). For experiments involving optogenetic activation combined with calcium imaging, MC4r-cre animals were injected in the LSS, employing the same coordinates as stated above, with a 1:1 mixture of pAAV5-hSyn-dlight1.2 and pAAV8-Ef1a-DIO-rsChRmine-oScarlet-WPRE (active opsin) or pAAV8-Ef1a-DIO-mScarlet-WPRE (control group). The following coordinates from bregma were used for optogenetic activation of NAcC (AP: 1,1; ML: ±1,5; DV: −4,1), medial NAc shell (AP: 0,8; ML: ±0,5; DV: −4,1), and dorsal striatum (AP: 0,8; ML: ±1,6; DV: −3,0). For fiber photometry in the NAcC the following coordinates were used: AP: 1,1; ML: ±1,5; DV: −4.1. For all virus injections, the injection needle was left in place for 10 min after injection to ensure proper diffusion. Following viral injections, animals were either implanted with an optic fiber implant or surgically closed with sutures. For optogenetic experiments, optic fiber implants (Doric Lenses Inc.; O.D. 5 mm, Fiber Core 200/250 μm, NA 0.66) were positioned 300 μm above the

injection sites. For fiber photometry, optic fibers (Doric Lenses Inc.; O.D. 5 mm, Fiber Core 400/430 μm, NA 0.66) were placed 100 μm above the targeted region. Optic fibers were fixed to the skull using dental adhesive resin cement (Super-bond C&B, Sun Medical co.) and black acrylic resin (Ortho-Jet, Lang Dental Manufacturing Co.). Analgesic treatment with Carprofen (5 mg/kg; Rimadyl, Pfizer) was administered during the first 48 h post-surgery. Animals were allowed to recover for at least 3 weeks after surgery to allow viral expression before conducting experiments. Prior to fiber-photometry experiments, the signal was screened and mice with very low signal-to-noise ratio were excluded. Following the behavioral experiments, construct expression, injection site, and fiber location were confirmed through fluorescent immunohistochemistry.

Fiber photometry

All fiber photometry measurements were conducted largely as previously described.[33] In short, fluorescent biosensors (GCaMP6s, GCaMP8m, dLight1.2, iGluSnFR) were excited at two wavelengths (465 nm and 405 nm for signal and isosbestic control, respectively) by light originating from two sinusoidally modulated LEDs (330 Hz and 210 Hz for 465 and 405 nm, respectively). The light was reflected off dichroic mirrors (5-ports fluorescence minicube; Doric Lenses, Inc) and passed on toward the optical implant of the mouse via a pigtailed 1 x 1 fiber optic rotary joint coupled to a low-autofluorescence fiber-optic patch cord (both 400 μm, 0.57 NA optical fiber; Doric Lenses, Inc). Light intensity was adjusted to 50 ± 10 μW (465 nm) and 25 ± 5 μW (405 nm), as measured at the tip of the patch cord. Emitted signals from both channels then returned through the same optical fiber cable and were acquired at 6.1kHz using a photosensor build into the fluorescence minicube, demodulated (lock-in amplification), filtered using a 6th order 6Hz low-pass filter, digitized at 1017.3 Hz, and recorded by a real-time signal processor (RZ5D; Tucker Davis Technologies). Timestamps of onset and offset of events occurring during the test were digitized by TTL input to the real-time signal processor from the behavioral test chambers (Med Associates, Inc).

Further offline analysis was performed using a custom-written Graphical User Interface (GUI) based on Python scripts as well as custom-written MATLAB scripts, and largely followed previously published analysis pipelines.[34,35] The raw 465nm and 405nm signals were down-sampled to 100 Hz. Next, to create peri-event plots, data was split into time bins comprising individual trials. Data for individual trials was then detrended to remove movement, photo-bleaching, and fiber bending artifacts. To this end, the 405 nm control signal was fitted to the 465 nm signal using linear polynomial regression. The change in fluorescence (dF) was then calculated by subtracting the predicted signal (fitted 405 nm signal) from the measured raw 465 nm signal, which subsequently was normalized through division by the predicted signal, resulting in dF/F (%).

Behavioral paradigms

Mice were habituated to handling and connection to a fiber patch cord for several days prior to the different test sessions.

Pavlovian fear-conditioning

For fear conditioning, mice were tethered to the photometry patch cable and placed in a mouse behavioral test chamber (Med Associates Inc.). Animals were exposed to a 30s tone (CS), and during the last 2s a 0.5 mA foot shock (US) was delivered via the grid floor of the test chamber. Animals were exposed to 6 trials. Inter-trial interval time was quasi-random with a mean of 3 min. On the following day, fear memory was tested by exposing the animals to 6 × 30s CS tones without foot shocks, in the same test chamber. Mice were videotaped during the conditioning and test session allowing quantification of body movement using the "Activity analysis" feature of EthoVision XT (Noldus). Thus, percentage of pixels changed per frame was calculated and used as a measure for body movement. Calcium activity (GCaMP8m) or release of dopamine (dlight1.2) or glutamate (iGluSnFR) was measured continuously throughout the entire session using fiber photometry. For correlating neural activity to body movements, fiber photometry signals were down-sampled to 10Hz and converted to % dF/F as described above. Next, we applied an iterative procedure (100 iterations, window size = 15s) to locally correct the signal for photobleaching and essentially create a signal with a flat baseline around '0%' throughout the entire session[35] We then performed a cross-correlation analysis between pixel changes in the video and the normalized fluorescent signal using the MATLAB function "xcorr" and a lag range of −10 to 10s.

To compare the neural response with and without D1-receptor-antagonism, animals were pretreated with either saline or SCH23390 hydrochloride (0.2 mg/kg, Tocris, Cat. No. 0925) dissolved in physiological saline and injected i.p. in a volume of 4 μL/g 20 min prior to fear conditioning described above. The following day, the animals were retested with the same conditions after pretreatment with the compound not administered on day 1. Maximal calcium transient height during the 2s shock was measured (in % dF/F) and compared between the 2 treatments.

Combined reward and aversion

Animals with GCaMP8m in MC4R-LSS neurons or dLight in the LSS area were trained in a Pavlovian conditioning where a 5s tone predicted a sugar pellet delivery (20 mg; Bio-Serv). Standard Med Associates test chambers were used together with custom, 3D-printed food-ports for allowing video recording of delivery and consumption of sugar pellets while the mice were attached to the fiber optic cable. The mice were food restricted to approximately 50% of their daily food intake for 3 nights before training started and kept at 85–90% of their initial body weight throughout the experiment. Mice were exposed to 5 training sessions consisting of 30 trials with quasi-randomized inter-trial intervals with a mean of 60s. On the sixth day, 10 of the 30 sugar pellet deliveries were unpredicted. On day 7, 10 of the trials were predicted by the tone but the pellet delivery was omitted. On day 8, the session started with 10 predicted pellet deliveries. The house light was then turned off and 10 foot shock trials predicted by 5s onset of cue-lights started. To compare the magnitude of GCaMP/dLight transients in response to sugar pellet consumption and foot shocks, as well as their respective cues,

videos of pellet trials were manually scored to mark the moment of pellet consumption. Maximal dF/F (%) within 2s surrounding pellet consumption, 2s following onset of the foot shock and during 2s pre-cue baseline for both conditions was measured. Peak values 1s before and 1s after cue onset were also measured. The mean peak dF/F was calculated for each condition for each animal. The peak dF/F value before cue onset was then subtracted from the maximal dF/F value after cue/event. Paired comparisons of responses to different conditions were performed.

Intracranial self-stimulation

Mice were connected to an optical fiber linked to a 460 nm LED source (Prizmatix Ltd.) and tested in a standard mouse test chamber (Med Associates Inc.). The chamber light was turned on to indicate the start of the test. The test chamber contained two nose-poke holes that were illuminated during the whole test. One of these holes was randomly paired to a 2s blue light stimulation (20 Hz, 10ms pulses, approximately 12 mW into the brain). When mice poked into the active hole, the port illumination ceased while the animal received the stimulation. Responses on the active hole during the 2 s stimulation period were recorded but did not lead to any additional stimulation. If the animal poked in the inactive hole, no stimulation was delivered, and the port remained illuminated. Each session lasted for 30 min and was performed for 3 consecutive days. The designation of the active port was changed daily.

Real-time place preference

A real-time place preference test was conducted one week after the completion of the intracranial self-stimulation test. A 3-chambered Panlab Spatial Place Preference Box (Harvard Apparatus) was used. On day 1, a pretest was conducted. Mice were connected to an optical fiber and allowed to move freely between the chambers of the box, to establish any specific preference. The chamber in which each mouse spent a lesser amount of time was designated as the non-preferred chamber. This non-preferred chamber was then coupled with blue light stimulation (20 Hz, 10ms pulses, approximately 12 mW into the brain) during the subsequent days of testing (days 2–4). For the testing phase (days 2–4), animals were attached to an optical fiber connected to a LED source. The animals were placed within the corridor of the apparatus and permitted to move freely through the chambers of the box. The animals received stimulation when in the light-paired chamber. All sessions were conducted for 15 min. EthoVision XT tracking software (Noldus) controlled animal location, and light stimulation in real-time Time spent in each chamber was measured to elucidate if the optogenetic activation establishes place-preference or aversion.

Locomotor activity

After the completion of the real-time place preference test, mice were tested for locomotor activity. For that, the animals were attached to an optical fiber connected to a LED source and placed in the center of an open-field arena (45 cm $\times$ 45 cm $\times$ 40 cm). Locomotion was assessed for 15 min: an initial 5 min free exploration without stimulation, followed by 5 min of 20 Hz blue light stimulation (10ms pulses, approximately 12 mW into the brain), concluded by 5 min of no stimulation.

Spontaneous locomotor activity was also evaluated in MC4r-cre mice with neuronal ablation pre- and post-injection of Casp3. Animals were placed in an open-field arena (45 cm $\times$ 45 cm $\times$ 40 cm) for 10 min.

Animals were monitored using a camera and EthoVision XT tracking software (Noldus). Total distance traveled was used to evaluate the effect of neural activation or ablation.

Voluntary wheel-running

Voluntary wheel-running activity was evaluated over two distinct time frames: a 10-day period prior to Casp3 injection and a subsequent 10-day period 3 weeks post-injection. Animals (n = 8 ablated, 8 controls) were single housed in filtertop cages (37 $\times$ 21 $\times$ 18 cm) and given continuous access to wireless running wheels. The quantification of wheel running behavior was conducted by tracking the number of wheel rotations over time. Data was exported and expressed as cumulative turns during each test period. During the whole experiment, food intake and body weight were measured at 3–4-day intervals. Measured food intake was divided by measurement interval and expressed as food intake per day.

Combined optogenetic activation and fiber photometry

Four weeks after surgeries, animals were placed in an operant chamber and connected to the optical fiber. During fiber photometry recordings, trains of either 2, 5, 10, 20 or 40 pulses of red light (625 nm, 20 Hz, 10ms pulse width, 5 mW from fiber tip) were delivered through the same fiber cable. The number of pulses administered in each trial was semi-randomly chosen from the 5 possible conditions, with a total of 10 trials per condition, i.e., 50 trials in total. We used a fixed intertrial interval of 45s. To quantify the dopamine released in response to the optical stimulation, area under the curve of the dF/F 3s before stimulation was measured and subtracted from the area under the curve 3s after stimulation. This measure was compared between the stimulation conditions. The following week, light intensity was titrated. This time, animals received 4 blocks of 10 stimulation trials (45s intertrial interval). In each trial, 5 pulses of red light (625 nm, 20 Hz, 10ms pulse width) were delivered, with the light intensity varying between trial blocks: 1 mW, 5 mW, 10 mW and 15 mW, measured from the fiber tip. The order of light intensities was randomly assigned to each animal. For each trial, the peak dF/F value following stimulation onset was identified. Next, per animal, the median of these peak values was derived for each of the 4 trial blocks. These medians were then used to compare the different light intensities.

Ex-vivo slice opto-photometry

Animals were bilaterally injected with a mixture of GCaMP8m or dLight1.2 combined with rsChrmine or mScarlet (rsChrmine in one hemisphere, mScarlet in the other hemisphere). At least 3 weeks later, animals were then anesthetized with 4% isoflurane. The brain was removed and transferred to ice-cold cutting solution saturated with 95% O_2 and 5% CO_2. Content of cutting solution (in mM): 92 NMDG, 20 HEPES, 25 glucose, 30 $NaHCO_3$, 1.2 NaH_2PO_4, 2.5 KCl, 5 sodium ascorbate, 3 sodium pyruvate, 2 thiourea, 10 $MgSO_4$, and 0.5 $CaCl_2$, pH 7.4. Coronal sections (300 μm) were cut using a vibratome (Leica). Sections were transferred to 35°C aCSF solution

for recovery (in mM): 125 NaCl, 2.5 KCl, 1.25 NaH_2PO_4, 1 $MgCl_2$, 11 glucose, 26 $NaHCO_3$, 2.4 $CaCl_2$ (310 mOsm, pH 7.4) saturated with 95% O_2, 5% CO_2. The aCSF with sections were placed at room temperature at least 30 min prior to recording. Sections were put in a recording chamber and perfused with fresh aCSF at a rate of 2 mL/min. Using a fluorescent microscope, transfected cells could be visualized. An optic fiber was placed in the bath above the fluorescent cells and fiber photometry recordings were performed as described above. To stimulate rsChrmine, five pulses of red light (625 nm, 20 Hz, 10ms, 23 mW from fiber tip) were used. GCaMP or dLight responses were measured during optical stimulation. Data was processed as described above.

Immunofluorescence

Animals were euthanized by CO_2 inhalation, transcardially perfused with 0.9% saline solution followed by 4% paraformaldehyde (PFA) in PBS (pH 7.4). Brains were removed, postfixed overnight in a 4% PFA solution, then transferred to a 30% sucrose-PBS solution until sinking. Brains were frozen in −80°C isopentane. Coronal sections of 40 μm were cut using a cryostat (Leica CM1959, Leica), then placed into a cryoprotectant buffer (composed of 0.1 M phosphate buffer, 30% ethylene glycol, and 20% glycerol), and stored at −20°C until further use. For free-floating immunofluorescent labeling, the sections were washed in PBS, followed by an incubation with blocking solution (1% BSA and 0.3% Triton X-100 in PBS). Subsequently, the sections were incubated overnight with primary antibodies diluted in blocking solution: rabbit anti-foxP2 (1:2000; Abcam, ab16046), rabbit anti-red fluorescent protein (anti-RFP, 1:1000; MBL International, PM005), chicken anti-GFP (1:10000; Abcam, ab13970). The sections were then washed in PBS and incubated for 2h with appropriate secondary fluorescent antibodies Alexa Fluor 488/568 (all obtained from Invitrogen): anti-rabbit (1:500; A21206; or 1:1000; A10042), or anti-chicken (1:1000; A11039). Finally, the sections were washed again with PBS, and mounted on glass slides using ProLong Glass Antifade Mounting agent (Thermofisher). Cells expressing MC4r-tdTomato were visualized without the use of immunohistochemistry. Sections were analyzed using a confocal microscope (Zeiss LSM 700, Carl Zeiss AG) or a widefield microscope (Leica DMi8) with 405, 488, 555, and 639 nm diode lasers. Confocal pictures were used for manually counting MC4R-LSS neurons co-expressing FOXP2 and D1 using ImageJ cell counter plugin.

RNA-Scope fluorescent in situ *hybridization*

Animals were transcardially perfused, and their brains removed, post-fixed, and cryoprotected in 30% sucrose, as described above. 16 μm brain sections were cut at the striatal level using a freezing microtome, mounted on SuperFrost Plus Gold slides (ThermoFisher), and baked at 60°C overnight. *In situ* hybridization was performed using RNAscope Multiplex Fluorescent assay v2 (Advanced Cell Diagnostics) following manufacturers' protocol. The mc4r probe (Cat No. 319181) was purchased from Advanced Cell Diagnostics (Newark). Pretreatment target retrieval was done at 98°C–99°C for 7 min, and sections were treated with Protease Plus for 22 min. Opal 570 tyramide (1:2000; Akoya Biosciences) was used to detect the MC4R probe. Microphotographs were obtained using a widefield microscope (Leica DMi8) at 25× magnification.

QUANTIFICATION AND STATISTICAL ANALYSIS

Statistics

GraphPad Prism 10 was used to make graphs and perform statistical analyses. Shapiro-Wilk tests were conducted to evaluate the normal distribution of the data. Two-tailed paired t-tests and one-sample t-tests were used when comparing two variables measured within the same subject and when comparing data for a single variable to a value of 0, respectively. When comparing more than two conditions, repeated measures ANOVAs followed by Šídák's multiple comparisons tests were used. Depending on the specific analysis, between-subject factors included opsin and nose pokes, while within-subject factors were time, light intensity, and stimulation duration. The interaction between these factors were also analyzed and stated. The data from the intracranial self-stimulation was not normally distributed. Thus, a logarithmic transformation of the data was applied before performing the ANOVA. Non-transformed data is still shown in the figures. Statistical tests used, as well as sample sizes, are stated in figure legends, the results section or in the supplemental statistical Table S1. Some data is descriptive and does not require statistical comparisons. Data is presented as mean, and error bars show SEM.